A new mass conservation approach to the study of CO_2 advection in an alpine forest

Leonardo Montagnani,[1,2] Giovanni Manca,[3] Elisa Canepa,[4] Emilia Georgieva,[5] Manuel Acosta,[6] Christian Feigenwinter,[7] Dalibor Janous,[6] Günther Kerschbaumer,[2] Anders Lindroth,[8] Luigi Minach,[2] Stefano Minerbi,[1] Meelis Mölder,[8] Marian Pavelka,[6] Günther Seufert,[3] Marcelo Zeri,[9,10] and Waldemar Ziegler[9]

Received 23 June 2008; revised 17 September 2008; accepted 21 January 2009; published 10 April 2009.

[1] A new method is proposed for the computation of CO_2 Net Ecosystem Exchange (NEE) and its components in a forest ecosystem. Advective flux is estimated by taking into account the air mass conservation principle. For this purpose, wind and dry air density values on the surface of the control volume are first corrected and then the advective flux is estimated on the surface of the control volume. Turbulent flux is also computed along the surface of the control volume while storage flux is computed inside the volume. Additional characteristics of this method are that incompressibility of the mean flow is not assumed a priori, and that vertical and horizontal advective fluxes are not treated separately, but their sum is estimated directly. The methodology is applied to experimental data collected with a three-dimensional scheme at the alpine site of Renon during the Advex project (July 2005). The advection flux was found to be prevailing positive at night and negative during the day, as was found in previous studies on advection for the same site, but showed a lower scatter in half-hour calculated values. We tested the effect of its summation on turbulent and storage fluxes to produce half-hourly values of NEE. Nighttime NEE values were used in functional relations with soil temperature, daytime values with PPFD. The effect of addition of the advection component was an increase in the values of parameters indicating ecosystem respiration, quantum yield, and photosynthetic capacity. The coefficient of correlation between NEE and environmental drivers increased.

Citation: Montagnani, L., et al. (2009), A new mass conservation approach to the study of CO_2 advection in an alpine forest, *J. Geophys. Res.*, *114*, D07306, doi:10.1029/2008JD010650.

1. Introduction

[2] In recent years, much information concerning interactions between forests and the atmosphere has been gained through micrometeorological techniques. In particular, the Eddy Covariance method (EC) has been applied to study both ecophysiological aspects of plants growing in different environments and to produce net annual carbon balance estimates [*Goulden et al.*, 1996]. These estimates are carried out taking into account only two terms of the mass conservation equation: vertical turbulent flux and storage flux, supposing that advection and horizontal turbulent flux are negligible [*Loescher et al.*, 2006].

[3] These assumptions can be applied to flat and homogeneous terrain [*Baldocchi et al.*, 1988]. However, a large percentage of temperate forested regions are in challenging terrain because of thousands of years of interaction with humans, with plains used for farming and settlements. As a consequence, much of the carbon absorbed or stored by forest ecosystems escapes proper quantification, since a reliable technique that takes into account advective fluxes occurring on sloping terrain is still not available.

[4] At night, when turbulence is not well developed, nonturbulent transport pathways may become important in nonhomogeneous environments resulting in a nighttime flux error in EC measurements that acts as a selective systematic error [*Moncrieff et al.*, 1996]. The impact of these errors on net CO_2 exchange and the estimation of carbon sequestra-

[1]Forest Services of Autonomous Province of Bolzano, Bolzano, Italy.
[2]Laboratory of Chemical Physics, Agency for the Environment of Autonomous Province of Bolzano, Bolzano, Italy.
[3]Climate Change Unit, Institute for Environment and Sustainability, Joint Research Centre, European Commission, Ispra, Italy.
[4]Department of Physics, University of Genova, INFM, CNISM, CNR, Genoa, Italy.
[5]Institute of Geophysics, Bulgarian Academy of Sciences, Sofia, Bulgaria.
[6]Institute of Systems Biology and Ecology, Academy of Sciences of the Czech Republic, Brno, Czech Republic.
[7]Institute of Meteorology, Climatology and Remote Sensing, University of Basel, Basel, Switzerland.
[8]Department of Physical Geography and Ecosystems Analysis, GeoBiosphere Science Centre, Lund University, Lund, Sweden.
[9]Max Planck Institute for Biogeochemistry, Jena, Germany.
[10]Energy Biosciences Institute, University of Illinois, Urbana, Illinois, USA.

0148-0227/09/2008JD010650

tion by the forest can be quantitatively important [*Massman and Lee*, 2002; *Loescher et al.*, 2006].

[5] The first advection estimates applied to the EC method were published by *Lee* [1998]. He proposed a computational method for the vertical advection term only, based on CO_2 concentration data collected by a single tower and wind data from a single anemometer placed above the canopy. This method was theoretically questioned by *Finnigan* [1999], who underlined the three-dimensional nature of the advective flux. However, *Baldocchi et al.* [2000], working over undulating terrain, compared it with chamber measurements and found that the vertical advection correction improved carbon balance estimates.

[6] *Aubinet et al.* [2003], *Feigenwinter et al.* [2004], and *Staebler and Fitzjarrald* [2004] first estimated horizontal advection on the basis of the direct measurements of the CO_2 concentration gradient, using a terrain-based coordinate system. Vertical advection was calculated using the Lee method. Later on, this approach was applied by *Marcolla et al.* [2005], *Yi et al.* [2008], and *Feigenwinter et al.* [2008].

[7] There are some important uncertainties in the quantification of advection terms [*Vickers and Mahrt*, 2006; *Heinesch et al.*, 2007]. Comparison of fluxes obtained by micrometeorological measurements (turbulent, advective and storage fluxes) with biological fluxes measured at night using independent methods, such as chamber-based modeling, has not yet been possible, because of the large variability in half-hourly advective fluxes [*Feigenwinter et al.*, 2004].

[8] The accurate estimate of the vertical wind component is difficult with available instrumentation. The methods developed to resolve this instrumental issue, such as the Lee method [*Lee*, 1998], the tilt angle method [*Paw U et al.*, 2000], the planar fit method [*Wilczak et al.*, 2001], and the divergence method [*Vickers and Mahrt*, 2006], which is dependent on the spatial scale over which the horizontal gradients used are calculated, lead to different vertical wind velocity estimates, both in absolute 30-min averages and in daily course values, and thus to different values of the vertical advection component.

[9] Estimation of the horizontal advection component is affected by assumptions on the position and shape of the reference volume used. In fact, it has been shown that variation in CO_2 source intensity may lead to concentration gradients along a slope [*Aubinet et al.*, 2005]. In addition, heterogeneity in leaf area density may influence air mixing [*Yi*, 2008] and hence local CO_2 concentrations.

[10] There is a point to underline concerning the coordinate reference system. While the source area of turbulent fluxes refers to an undefined volume with a projection on the ground that is teardrop shaped, more or less lengthened upwind as a function of atmospheric stability, advective flux estimations have been calculated up to now with a defined reference system, both in 2-D [*Aubinet et al.*, 2003; *Marcolla et al.*, 2005] and 3-D cases [*Feigenwinter et al.*, 2004; *Staebler and Fitzjarrald*, 2004; *Turnipseed et al.*, 2004; *Feigenwinter et al.*, 2008]. Since, as pointed out by *Finnigan* [2004a, 2004b], it is fundamental to define a unique reference system for all mass balance terms, a comprehensive equation is needed to define NEE in a univocally defined space with a single reference system for all flux terms.

[11] In this paper, we focus on a theoretical framework allowing better estimation of advective fluxes in conditions of topographically complex terrain. For air pollutant dispersion modeling in such conditions the air mass conservation principle is of primary importance, as was shown already in the late 1970s [*Sherman*, 1978]. In fact, small errors in air density and wind fields may induce large errors in trace gas source or sink estimates [*Byun*, 1999; *Lee et al.*, 2004]. We believe that the requirement of air mass conservation in the control volume is important also for the computation of CO_2 advective fluxes in hilly terrain. Thus, the approach proposed here is based on the air mass conservation principle.

[12] Moreover, the method presented for NEE estimations differs from those used previously since it uses a single reference system: advective fluxes are computed with an Eulerian approach on surface elements of the control volume instead of being computed inside the control volume, with separated computations for horizontal and vertical advection components.

[13] The objective of this study is to propose a new methodology for advective flux computation, and to demonstrate its performance by adding the obtained values to turbulent and storage fluxes computed following a more traditional approach. We have used data from the first year of measurements of the Advex extensive field campaign performed to study the nonturbulent transport of CO_2 at three European forest sites [*Feigenwinter et al.*, 2008]. In section 2 the characteristics of the study area where measurements were carried out are presented; in section 3 the experimental setup is described; in section 4 the proposed theory and calculation methods are explained; in section 5 the results are discussed.

2. Site Description: Orography, Vegetation, and Wind Regime

[14] The study site is Renon-Selva Verde (46°25′ N, 11°17′ E, elevation about 1735 m asl), part of the CarboEurope-IP network (data available at http://gaia.agraria.unitus.it/database). It is located in northeast Italy, on the southern side of the Alps at a distance of 12.2 km north-northeast from the town of Bolzano. The site is placed on a porphyric plateau that is part of the irregular slopes of "Cima del Lago Nero" (2069 m) and is between the wide Isarco river valley and the narrow and steep Sarentino river valley (Figure 1a). The nearest peaks are "Corno di Renon" (2259 m asl) at about 3.7 km north-northeast and "Cima di Villandro" (2509 m asl) at about 8.2 km north-northwest.

[15] The site vegetation is of natural origin and is used for wood production. It consists of an unevenly aged coniferous forest with gaps between groups of older and younger trees. The main forest species is spruce (*Picea abies* (L.) Karst., 85% in number) followed by cembran pine (*Pinus cembra* L., 12%) and larch (*Larix decidua* Mill., 3%). Reported net ecosystem production is 450 gC m^{-2} a^{-1} [*Valentini et al.*, 2000]. In the area chosen as reference (see Figure 1b) different forest types are present: mesophilous mature forest covers 52.3% of the surface, waterlogged mature forest 21.0%, young forest 12.0%, while clearings cover 14.7% of the area. The canopy is irregular with maximal height of 29 m in the reference area. The mean leaf area index (LAI), measured by hemispherical photographs [*Cescatti*, 2007] is

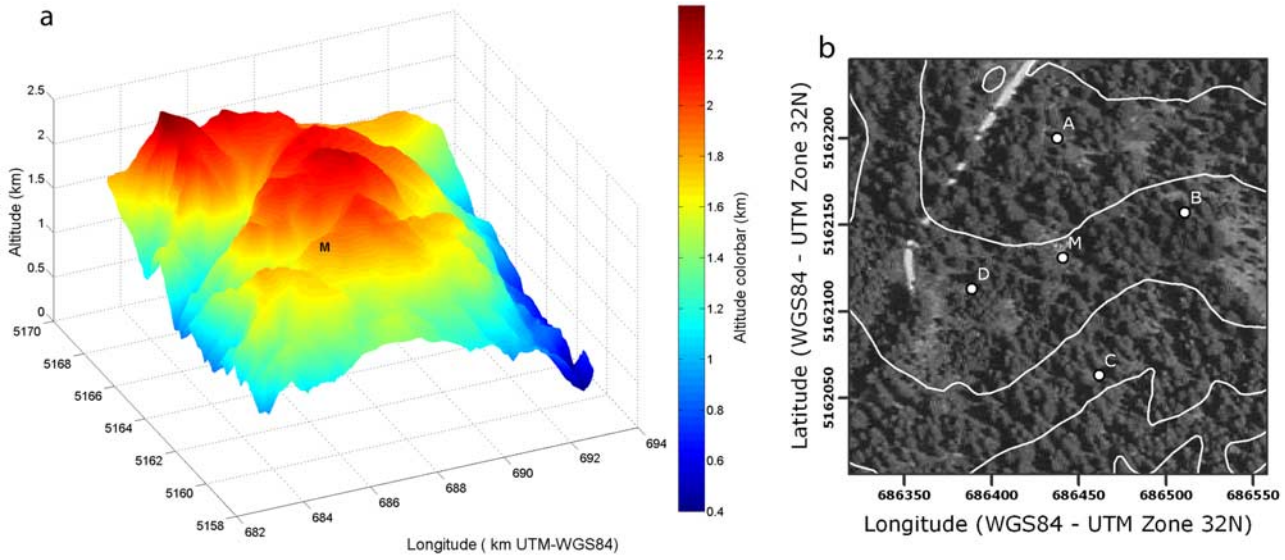

Figure 1. (a) The Renon site (M) is at the southern slope of the Alps in South Tyrol (Italy). The area represented is 10 × 10 km. (b) Plan view of the site during the Advex campaign. Letters A, B, C, D, and M refer to meteorological towers defining the reference area; the area represented is 240 × 240 m.

5.1 m^2 m^{-2}. The leaf area density, measured along the measurement towers, showed two peaks: the first at understory level, the second at 2/3 of maximal canopy height. Outside the reference area, at a distance of 80 m northwest of the central tower (point M on Figure 1), tree density decreases and the forest is replaced by ample pastures with sparse trees.

[16] The typical synoptic situations and the prevailing winds for northeast Italy were analyzed on the basis of NCAR/NCEP reanalysis [*Kalnay et al.*, 1996] and on standard meteorological observations in the region of Bolzano. Two main large-scale flow patterns that lead to the following predominant winds in the study area have been identified: (1) winds coming from north or northwest, which is frequent during winter and only occasional during summer; (2) persistent winds coming from the south, which is typical for low-pressure systems located over the western Mediterranean area. When synoptic forcing is small or missing, winds in the area are driven by local forcing and thus mountain valley winds prevail. This occurs especially in summer, when temperature gradients are higher than in winter. In this case, winds are from the north during the night and from the south or southwest (i.e., from the Bolzano town plain) during the day.

3. Experimental Setup and Measurements

3.1. Advection Experimental Setup

[17] Four external towers (A, B, and D were all 30 m high, while C was 41.5 m high), arranged to form an irregular quadrilateral area around a permanent central tower (M, 42 m high), constituted the experimental design of the Advex campaign, which ran from 1 May to 15 September 2005, but only data from July are used here. Two of the towers, B and D, were placed at the same elevation, 1733 m asl, while the other two, A and C, were placed at 1745 and 1720 m asl, at approximately the maximum and the minimum elevation of the reference area, respectively (Figure 1b). The area enclosed within the four external towers was about 8900 m^2; this area is intended to be the projection of the base of the control volume (Figure 2) on a plane perpendicular to local gravity. The distances between the towers were AB ∼ 84.8 m, BC ∼ 106.5 m, CD ∼ 88.5 m, and AD ∼ 99.6 m. The maximum slope was 17.83% at an azimuth of 169°98′ N; the mean inclination was 16.82% southward and 5.85% eastward. The trees reached 29 m at towers B and C, 25 m at tower A, while towers M and D were sited in clearings. Temperature, wind velocity, the CO_2 and H_2O molar fractions were measured at each external tower at four levels: 1.5 m, 6 m, 12 m and 30 m above ground level (agl). Additionally, at tower C, wind velocity was measured at a level of 41.5 m agl. All measured variables are listed in Table 1.

[18] Air temperature was measured by means of 75 μm unscreened chromium-constantan thermocouples, type E (FW3-Campbell Scientific Incorporated, Logan, Utah, United States; CSI hereafter). All thermocouples were connected via an AM25T multiplexer (CSI) to a dedicated data logger (CR 23x, CSI) in order to have the same reference temperature. Data were collected at a frequency of 0.5 Hz.

[19] Anemometric data were collected at a frequency of 10 Hz by three-dimensional sonic anemometers: (1) model 81000V, RM-Young, Michigan, United States, at towers A, B, and D at 1.5 m, 6 m, 12 m, and 30 m and at tower C at 1.5 m agl; (2) model R3, Gill Instruments, Lymington, United Kingdom, at tower C at 6 m, 12 m, 30 m, 41.5 m agl. The data from the anemometers placed at each tower were converted into net signals at the tower's base and then transmitted via optic fibre to an industrial PC for data acquisition. Besides this wind measurement system, data coming from four additional anemometers placed on the central tower M (81000V, RM-Young, Michigan, United States) at 1.5 m, 6 m, 12 m agl, and Gill HS, Gill Instruments, Lymington, United Kingdom, at 32 m agl were collected and used in this study. All anemometers were

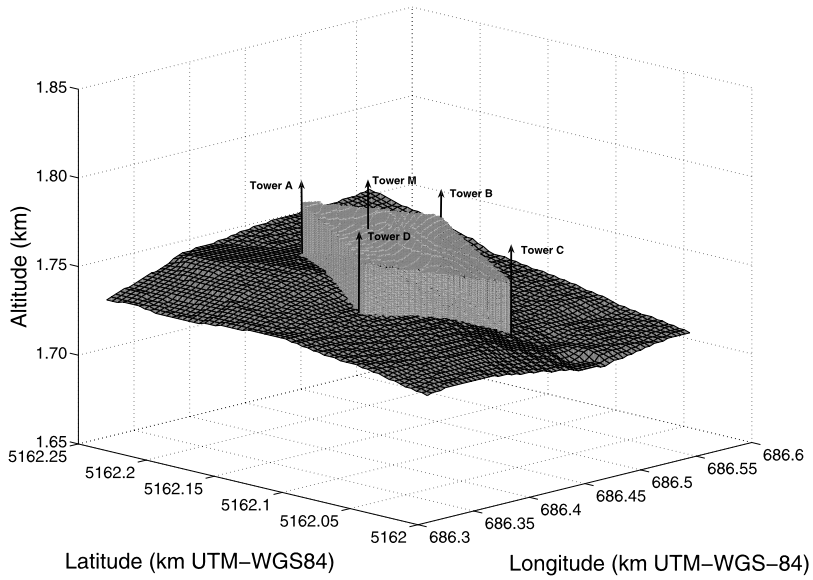

Figure 2. Control volume (gray box) over the local topography (dark gray surface) of Renon. Arrows show the location of towers A, B, C, D, and M. The dark gray area represents the soil surface represented in Figure 1b, 240 × 240 m.

aligned with local gravity to within about 1° with the aid of an inclinometer. The azimuth was calculated by sighting a geographical object. Regular Cartesian coordinates were used, which refer to the Earth and are time- and space-independent, and have the advantage of coordinating multiple sonic anemometers and trace gas observations [*Sun*, 2007].

[20] *Loescher et al.* [2005] have shown that the Gill R3 and RM-Young 81000V anemometers have similar behavior due to the physical geometry of the instruments, but the lack of complete sonic anemometer intercalibration leads to measurement uncertainties in this study. Additional uncertainties may arise from the alignment of the vertical axis of the anemometers [*Sun*, 2007] as well as from local leaf drag influence on wind components.

[21] In order to measure the CO_2 and H_2O molar fractions, air was sampled by polyethylene tubes of 4 mm inner, and 6 mm external diameter (Festo, Esslingen, Germany) from inlets placed at the heights of the anemometric measuring points. Air was sampled by two independent systems, both consisting of two vacuum pumps: one of them was used for air sampling from all the lines, the other was used for the sampled line only [*Xu et al.*, 1999]; both pumps had a 15 l min^{-1} flow range. Two programmable systems were set up to sample line selection by 3-way solenoid valves (Type 6014, Bürkert, Ingelfingen, Germany). Each system sampled nine points: one common reference point placed at the base of the main tower used for intercalibration of the closed-path analyzers, and eight measuring points. One system sampled the air at 1.5 m agl and 12 m agl; the other at 6 m agl, and 30 m agl on each of the four external towers. Sampling time of each line was set to 40 s, giving five measuring cycles for each point every 30 min. Two closed-path analyzers (LI-6262, LI-COR, Lincoln, Nebraska, United States) were used. The two analyzers were pressure-controlled and placed at the same temperature (range 20–25°C). The CO_2 and H_2O molar fractions were obtained from recorded values of voltage (mV), cell temperature (K), and pressure (kPa). All data were collected on the central PC; the first 15 s of air sampling were discarded from half-hour average computation in order to allow a complete air change within the IRGA cell.

[22] The CO_2 dry molar fraction $\overline{r}_c$ was calculated from the CO_2 molar fraction $\overline{r}_{cmoist}$ and the H_2O molar fraction $\overline{r}_{wmoist}$ by the following equation:

$$\overline{r}_c = \frac{\overline{r}_{cmoist}}{1 - \overline{r}_{wmoist}} \tag{1}$$

The choice of using two analyzers to measure CO_2 and H_2O vertical profiles was made in order to minimize the uncertainty in half-hourly averaged values due to sampling

Table 1. Sensors Installed During the Advex Campaign

Locations	Sensors	Height (m agl)	Manufacturer	Model
Tower A	CO_2/H_2O	1.5, 6, 12, 30	LI-COR	LI 6262
	air T	1.5, 6, 12, 30	Campbell	FW3
	u, v, w	1.5, 6, 12, 30	RM-Young	81000V
Tower B	CO_2/H_2O	1.5, 6, 12, 30	LI-COR	LI 6262
	air T	1.5, 6, 12, 30	Campbell	FW3
	u, v, w	1.5, 6, 12, 30	RM-Young	81000V
	CO_2/H_2O	soil	LI-COR	LI 8100-101
	CO_2/H_2O	0.4, 0.9, 1.5, 3, 6, 9, 12, 15.5, 19, 22.5, 26.5, 30.5	LI-COR	LI 7000
Tower C	CO_2/H_2O	1.5, 6, 12, 30	LI-COR	LI 6262
	air T	1.5, 6, 12, 30	Campbell	FW3
	u, v, w	1.5	RM-Young	81000V
	u, v, w	6, 12, 30, 41.5	Gill	R3
Tower D	CO_2/H_2O	1.5, 6, 12, 30	LI-COR	LI 6262
	u, v, w	1.5, 6, 12, 30	RM-Young	81000V
	air T	1.5, 6, 12, 30	Campbell	FW3
Tower M	u, v, w	1.5, 6, 12	RM-Young	81000V
	u, v, w	32	Gill	HS
	CO_2/H_2O	32	LI-COR	Li 7500
	Net radiation	38	Kipp & Zonen	CNR1
	PPFD	38	Delta-T	BF2
	Pressure	1.5	Campbell	CS 105

frequency. *Heinesch et al.* [2007] showed that a minimum of five repetition cycles in the half-hour is needed to keep the uncertainty of CO_2 concentration measurements below 2 ppm under stable conditions or below 1.2 ppm under unstable/weakly stable conditions. However, the use of different instruments gives rise to the question of intercalibration. In the present study, two precautions were used to avoid fictitious concentration gradients. First, each analyzer measured air sampled along two planes placed at the same height above ground, formed by four sampling points each; second, a common point at 1.5 m agl at the central tower (M) was used to check on the accuracy of intercalibration and to allow postprocessing adjustment.

[23] Even though the same model of instrument (LI-6262) was used, a significant drift was observed in one of the analyzers during the month of June 2005. This month was excluded from further analyses in the present study. At the beginning of July 2005 a new LI-6262 analyzer was installed. The two LI-6262 analyzers showed a relative drift below 1 μmol mol^{-1} over 5 days. During postprocessing a further reduction in the discrepancy between analyzer outputs was attained by minimizing the zero offset by a linear relation. After this correction, the difference in half-hourly averaged data collected at the common point was (mean ± SD) 0.0017 ± 0.83 μmol mol^{-1}.

[24] Nitrogen (produced by Messer, Milano, Italy) was used to set the zero at the reference cell of analyzers. The analyzers were calibrated at the same time every 5 days. The same nitrogen flask was used to set the zero, the H_2O span was set by a Li 6100 dew-point generator (LI-COR), the CO_2 span was set by a 369-ppm flask (Messer, Milano, Italy).

[25] For analysis of the collected data, half-hourly averages of the measured variables were used following other advection studies for different CarboEurope sites [e.g., *Feigenwinter et al.*, 2004; *Aubinet et al.*, 2005] or Ameriflux sites [e.g., *Turnipseed et al.*, 2003] although a contribution to the turbulent flux can be given by air motions with timescales larger than this averaging period [*Finnigan et al.*, 2003].

[26] In order to perform the present study, we considered unambiguously valid data only. Rainy periods were excluded because water droplets in the optical path affect the performance of open path analyzers, as well as overall accuracy of both sonic anemometers (particularly the RM-Young 81000V) and thermocouples. Furthermore, all half-hourly data collected when at least one sensor was not properly functioning, or instrumentation was under calibration or maintenance, were excluded. Therefore, our analysis focused on the month of July 2005, which was the period when the instruments produced the highest percentage (77%) of valid data.

3.2. Complementary Measurements

3.2.1. Eddy Covariance

[27] Turbulent flux measurements with the EC technique were performed at the permanent central tower following the Euroflux methodology [*Aubinet et al.*, 2000]. Measurements were performed at a height of 32 m agl by a Gill HS anemometer and a LI-7500 (LI-COR) CO_2/H_2O open-path analyzer.

[28] Eddy fluxes were calculated using EDDYSOFT software [*Kolle and Rebmann*, 2007; *Mauder et al.*, 2008]: (1) no detrending, no high or low-pass filtering corrections were used; (2) a two-axis rotation of coordinates was applied each 30 min; and (3) the WPL corrections were performed [*Webb et al.*, 1980]. The software automatically calculated the lag time for CO_2 at each half-hour to maximize the covariances between fluctuations in vertical wind velocity and gas mole density. During the month of July 2005 it was 0.20 ± 0.15 s (mean ± SD). In addition, the analysis of stationary conditions for CO_2 turbulent flux and of Integral Turbulent Characteristic (ITC) following *Foken and Wichura* [1996] was performed. As a result, half-hours for which theoretical concerns existed on Reynolds decomposition because of lack of stationarity or for which the turbulence was not well developed and not suitable for further detailed analyses [*Göckede et al.*, 2008] were flagged for their recognition. Conditions of nonstationarity (30% maximum difference allowed) were found in 27.2% of the cases, while periods having inadequate integral turbulent characteristics were 12.8%. Data having both shortcomings were 4.4%. After quality check of the measurements, flux values collected during nonstationary periods or during periods of not well-developed turbulence, a total of 35.6% of the data, were excluded in the analysis of functional relations between NEE and environmental constraints (see section 5.6).

3.2.2. Additional CO_2 and H_2O Vertical Profiles

[29] The CO_2 and H_2O molar fractions were additionally measured at tower B at 12 levels: 0.4 m, 0.9 m, 1.5 m, 3 m, 6 m, 9 m, 12 m, 15.5 m, 19 m, 22.5 m, 26.5 m and 30.5 m agl. Air was sampled at each sampling line by 12 single pumps sited along the lines [*Mölder et al.*, 2000]. The CO_2 and H_2O molar fractions were measured by a dedicated LI-7000 (LI-COR). Data were stored on a logger (CR23x, CSI).

[30] The comparison between the 12-point profiles measured at tower B and the profiles measured at the same location by the main system highlighted a problem in the latter. A leak from the sampling polyethylene tube system collecting air from the 12 m measurement level at the four lateral towers was detected, therefore these data had to be excluded from further computations.

3.2.3. CO_2 Efflux From the Soil

[31] The CO_2 efflux from the soil (SR) was found to be heterogeneous both in time and space in previous studies performed at the site [*Janssens et al.*, 2003; *Rodeghiero and Cescatti*, 2005, 2008]. For the purposes of the Advex campaign, SR variability was measured by means of two different types of nonsteady state closed dynamic systems.

[32] The spatial distribution of CO_2 sources at ground level inside the reference area was measured in the context of a more extensive measurement campaign, carried out in the footprint known for the site [*Rebmann et al.*, 2005]. Five hundred and fifty-six CO_2 efflux measurements were made from day 193 to 195 using three identical systems working simultaneously. The systems were developed at the Institute of Systems Biology and Ecology, Czech Republic [*Pavelka et al.*, 2007]. Each system consisted of an LI-6250 analyzer (LI-COR), operating in closed mode with a dark soil PVC chamber. Each soil chamber had a volume of 3167 cm^3 and was equipped with a pressure equilibrium vent and small

fan for gentle air mixing. Measurements were made on 42 PVC collars (diameter 19.5 cm and height 8.5 cm), arranged in groups of three, inserted in the soil to a depth of 3 cm.

[33] Temporal variability in the CO_2 efflux from the soil was measured during the whole month of July by means of an automated chamber (LI-8100-101, LI-COR) [*Xu et al.*, 2006] placed near tower B where the vegetation type was intermediate between waterlogged and mesophilous forest. Collar size and diameter were the same as those used for LI-6250 (LI-COR) analyzers. Measurements were performed every 30 min. Sampling time was 120 s with the first 30 s set as a dead period, therefore effective sampling time was 90 s. A measured CO_2 molar fraction value was collected every second. CO_2 efflux from the soil was calculated based on the measured CO_2 molar fraction inside the chamber and with application of a linear interpolation for the temporal variation.

3.2.4. Meteorological Measurements

[34] We used long-term data on soil temperature, surface pressure and radiation collected in the framework of the CarboEurope IP project (http://gaia.agraria.unitus.it/database/newvars.asp) and stored on a central data logger (CR23x, CSI). The collection interval was 30 min.

[35] Soil temperatures (T_{soil}) were measured in each of the four vegetation types (section 2) at a depth of 0.05 m by PT100. Pressure values were measured at a single point in the reference area, at the meteorological station placed near the base of the central tower (1737 m asl) by a CS 105 (CSI). Net radiation (longwave and shortwave components) was measured at the central tower M at 38 m agl by a CNR1 (Kipp and Zonen, Delft, Netherlands). At the same location, Photosynthetically active Photon Flux Density (PPFD) was measured by a BF2 sunshine sensor (Delta-T Devices, Burwell, Cambridge, United Kingdom).

4. Methods

4.1. Theoretical Background

[36] The instantaneous transport and diffusion equation for a nonbuoyant scalar (CO_2) released in the atmosphere and dispersed by bulk air motions, neglecting molecular diffusion, is

$$\chi = \frac{\partial n_c}{\partial t} + \nabla \cdot (n_c\, \mathbf{u}) \tag{2}$$

where χ represents the rate of change in mole density with time t due to the presence of sources and/or sinks, n_c is CO_2 mole density, ∇ is the gradient operator $\nabla = \mathbf{i}\frac{\partial}{\partial x} + \mathbf{j}\frac{\partial}{\partial y} + \mathbf{k}\frac{\partial}{\partial z}$, with **i**, **j**, **k** being unitary vectors for the Cartesian coordinates with eastward as x, northward as y, and upward normal to the geopotential surface as z directions, and **u** is the instantaneous wind velocity vector, with wind components **u** (u, v, w) respectively.

[37] The mean transport and diffusion equation is obtained by Reynolds averaging of the instantaneous equation (2):

$$\chi = \frac{\partial \overline{n}_c}{\partial t} + \nabla \cdot (\overline{n}_c\, \overline{\mathbf{u}}) + \nabla \cdot \left(\overline{n'_c\, \mathbf{u}'}\right) \tag{3}$$

where the overbars indicate time averaged quantities and primes indicate fluctuations around the average of the corresponding quantities. The term $\frac{\partial \overline{n}_c}{\partial t}$ represents the time rate of change of the mole density; the term $\nabla \cdot (\overline{n}_c\, \overline{\mathbf{u}})$ represents the mean or advective flux divergence and the term $\nabla \cdot \left(\overline{n'_c\, \mathbf{u}'}\right)$ represents the divergence of eddy flux.

[38] Equation (3) can be rewritten as

$$\chi = \frac{\partial \overline{n}_c}{\partial t} + \overline{u}\frac{\partial \overline{n}_c}{\partial x} + \overline{v}\frac{\partial \overline{n}_c}{\partial y} + \overline{w}\frac{\partial \overline{n}_c}{\partial z} + \overline{n}_c\left(\frac{\partial \overline{u}}{\partial x} + \frac{\partial \overline{v}}{\partial y} + \frac{\partial \overline{w}}{\partial z}\right) + \frac{\partial \overline{u'n'_c}}{\partial x} + \frac{\partial \overline{v'n'_c}}{\partial y} + \frac{\partial \overline{w'n'_c}}{\partial z} \tag{4}$$

The CO_2 conservation equation is sometimes expressed in terms of mixing ratio [e.g., *Paw U et al.*, 2000; *Massman and Lee*, 2002; *Leuning*, 2007], since it is a conserved quantity [*Kowalski and Serrano-Ortiz*, 2007]. However, we maintain the scalar conservation formulation in terms of CO_2 density, as used in the FLUXNET community [*Aubinet et al.*, 2000] in order to highlight the corrections we are proposing in the estimations of NEE.

[39] Comparing equation (4) to the mass conservation equation commonly applied in the FLUXNET community [e.g., *Feigenwinter et al.*, 2004], the main assumptions made in previous studies on CO_2 flux computation are to be recalled: the assumption of incompressible mean wind field ($\frac{\partial \overline{u}}{\partial x} + \frac{\partial \overline{v}}{\partial y} + \frac{\partial \overline{w}}{\partial z} = 0$), as well as the assumption of neglecting the horizontal turbulent flux divergence terms ($\frac{\partial \overline{u'n'_c}}{\partial x} = \frac{\partial \overline{v'n'_c}}{\partial y} = 0$). Different authors [e.g., *Finnigan*, 1999; *Paw U et al.*, 2000] highlight that these assumptions have to be revised in certain cases, especially for heterogeneous canopy conditions. Therefore we used as a basis the general mean transport and diffusion equation (3).

[40] Equation (3) is an expression for the mass conservation of the average concentration at a fixed point. In practice, we are interested in the mass balance in a control volume built over a representative surface area, therefore we integrate equation (3) over a control volume V whose lower boundary is the area under investigation:

$$\iiint_V \chi\, dV = \iiint_V \frac{\partial \overline{n}_c}{\partial t} dV + \iiint_V \nabla \cdot (\overline{n}_c\, \overline{\mathbf{u}}) dV + \iiint_V \nabla \cdot \left(\overline{n'_c\, \mathbf{u}'}\right) dV \tag{5}$$

After applying the Gauss theorem, equation (5) becomes

$$\iiint_V \chi\, dV = \iiint_V \frac{\partial \overline{n}_c}{\partial t} dV + \iint_S n_c\, \overline{\mathbf{u}} \cdot d\mathbf{S} + \iint_S \overline{n'_c \mathbf{u}'} \cdot d\mathbf{S} \tag{6}$$

$$I \qquad II \qquad III \qquad IV$$

where S is the total surface of the control volume, and $d\mathbf{S}$ is a unit vector pointing outward from the surfaces of the control volume.

[41] In equation (6) *I* is the NEE of the scalar term; *II* is the change in storage term; *III* is the advection term; *IV* is the turbulent transport term.

[42] As in the local version of the scalar conservation equation, equation (3) or (4), in the integral version of the same equation, equation (6), the assumptions of air incom-

pressibility and negligible horizontal turbulent flux divergence are not necessarily satisfied.

[43] Calculation of CO_2 average mole density from CO_2 average dry molar fraction values (section 3.1) can be obtained by the product $\overline{n}_c = \overline{r}_c \overline{n}_{tot}$, where $\overline{n}_{tot}$ is the average total mole density of dry air. Therefore the advection term *III* becomes

$$\text{Term } III = \iint_S \overline{r}_c \, \overline{n}_{tot} \, \overline{\mathbf{u}} \cdot d\mathbf{S} \tag{7}$$

In practice, we have measurements only at a few points in the control volume so we must add extra information to calculate this term. In the present study we apply algorithms for the reconstruction of the 3-D CO_2 molar fraction, the mole density of dry air and the wind fields starting from available tower measurements (see section 4.3).

[44] However, data used for calculations may have mass conservation problems due to various causes, such as the representativeness of the measurement points, instrumental errors, improper space discretization procedures, or errors introduced by the interpolation algorithms. Therefore, it is to be expected that the mole density of dry air and wind field may not satisfy mass conservation accurately. Evidently, before performing CO_2 advective flux computations, air density and wind field have to be corrected for mass conservation.

[45] The mass continuity equation for dry air is

$$\frac{\partial \rho_{dry}}{\partial t} + \nabla \cdot \left(\rho_{dry} \mathbf{u} \right) = 0 \tag{8}$$

where $\rho_{dry} = m_{dry} n_{tot}$, with m_{dry} = molecular mass of dry air (kg mol^{-1}). Assuming m_{dry} as a constant, equation (8) reduces to

$$\frac{\partial n_{tot}}{\partial t} + \nabla \cdot (n_{tot} \mathbf{u}) = 0 \tag{9}$$

which after Reynolds decomposition and averaging can be rewritten in the form

$$\frac{\partial \overline{n}_{tot}}{\partial t} + \nabla \cdot (\overline{n}_{tot} \overline{\mathbf{u}}) + \nabla \cdot \left(\overline{n'_{tot} \mathbf{u}'} \right) = 0 \tag{10}$$

[46] At this point we will concentrate on the second term expressing the divergence of the mean airflow. The estimation of this term, $\nabla \cdot (\overline{n}_{tot} \overline{\mathbf{u}})$, for practical purposes is influenced by a "spurious" divergence introduced by the interpolations techniques applied, the inaccuracy of the measurements and their representativeness. We suppose that this spurious divergence is in general greater than $\frac{\partial \overline{n}_{tot}}{\partial t}$ and $\overline{n'_{tot} \mathbf{u}'}$, terms that we will assume as negligible. Following this approximation, equation (10) reduces to

$$\nabla \cdot (\overline{n}_{tot} \, \overline{\mathbf{u}}) = 0 \tag{11}$$

The above equation will be used to correct for mass conservation the product of the total mole density of dry air and wind (for more details see section 4.4). It is to be noted that this form of the continuity equation allows the average total mole density of dry air to be inhomogeneous. For example, in terrains with heterogeneous vegetation or rolling slopes unevenly exposed to the sun, horizontal temperature gradients may induce variability in the average total mole density of dry air.

[47] The approach we are proposing in this study differs significantly from what is commonly applied in advection estimates, e.g., *Feigenwinter et al.* [2008], since (1), we do not assume a priori the incompressibility of the mean flow, but compute dry air density on the basis of measured air temperature, pressure and water vapor mole density; (2), we do not compute the fluxes along gradients, but use measured values of CO_2 dry mole density and wind velocity; (3) we do not apply rotations to coordinates, but use regular Cartesian coordinates; (4) we implement an algorithm for air mass conservation before proceeding with flux calculations; (5) we do not treat separately vertical and horizontal advective fluxes, but compute their sum from values estimated on surface elements of the control volume.

4.2. Control Volume

[48] A control volume has to be defined in order to calculate the terms of the transport and diffusion equation for CO_2 concentration. The choice of its width and shape is arbitrary, but it must be representative of the ecosystem studied by the EC measurements.

[49] In this study, the control volume (Figure 2) is defined as an irregular four-sided volume of 267030 m^3 confined at the bottom by the terrain, laterally by four vertical plane surfaces (each of which is placed between adjacent measurement towers), and at the top by a sloping plane intersecting towers A, B and C at 30 m agl. The D and M towers are intersected at 29.7 m and 27.7 m, respectively, because of small-scale unevenness of the terrain (all these heights are below the height of the uppermost measurement point). For numerical calculations, a spatial discretization of 1 m was used with a mesh of 1 m both in the vertical and horizontal directions.

4.3. Three-Dimensional Fields of the Physical Quantities of Interest in the Control Volume

[50] In order to calculate the advection term, see equation (7), we need to know the values of the three physical quantities of interest: total mole density of dry air, $\overline{n}_{tot}$, the CO_2 dry molar fraction, $\overline{r}_c$, and wind velocity, $\overline{\mathbf{u}}$, averaged for each 30-min interval and for each cell of the control volume. For the reconstruction of the 3-D fields of the above quantities, starting from the available tower measurement, two different interpolation algorithms were applied on the basis of the shape of the measured profiles (see section 5.2).

[51] 1. Total mole density of dry air: The 3-D fields of total mole density of dry air were obtained from the measured values of air temperature, air pressure and the H_2O molar fraction inside the control volume. Temperature and the H_2O molar fraction were measured at three levels at each external tower (1.5 m, 6 m, and 30 m agl). Pressure data were collected only at the base of the central tower, thus to calculate air pressure values at the same points where air temperature and the H_2O molar fraction were measured a vertical pressure profile for each 30-min interval was constructed by extrapolating surface data in the vertical

with a linear decrease of 10 Pa m^{-1}. This pressure profile was then assumed to be valid for the entire control volume. As a further step, the total mole density of dry air, $\overline{n}_{tot}$, was calculated for each measurement point by the following equation based on Dalton's law of partial pressures:

$$\overline{n}_{tot} = \frac{\overline{p}_a - \overline{e}}{R\overline{T}_a} \tag{12}$$

where $\overline{p}_a$ is the air pressure, R is the universal gas constant, $\overline{T}_a$ is the air temperature, $\overline{e} = \overline{p}_a\,\overline{r}_{wmoist}$ is the vapor pressure, and $\overline{r}_{wmoist}$ is the H_2O molar fraction. For each lateral tower the vertical profile of the total mole density of dry air, n_{tot}, was calculated with a resolution of 1 m using a polynomial second-order equation fit. A log-log function was used to perform a nonlinear transformation to increase linearity between measured variables:

$$\ln h = a(\ln \overline{n}_{tot})^2 + b(\ln \overline{n}_{tot}) + c \tag{13}$$

where h is the height agl, and a, b, c are interpolation parameters for each half-hour. The 3-D air density field was obtained through horizontal interpolation of the vertical profiles. A linear interpolation based on a Delaunay triangulation of the data was applied. The Delaunay triangulation was computed using the Quickhull algorithm [*Barber et al.*, 1996]. Each triangle was a plain surface and the vertices of each triangle were points of the four vertical profiles calculated by the procedure described above.

[52] 2. The 3-D CO_2 dry molar fraction fields: For the CO_2 3-D field the same sampling heights and interpolation algorithms applied for n_{tot} were used.

[53] 3. The 3-D wind fields: Data from all meteorological towers were used to obtain the 3-D half-hourly averaged wind fields in the control volume. As a first step, vertical profiles with 1 m resolution were obtained at the towers using linear interpolation of the wind components (u, v, w) between the levels of measurements (see section 3.1). Below the lowest observation level the wind components were assumed to decrease linearly to zero at ground level. For the purposes of comparison we also calculated vertical profiles as proposed by *Feigenwinter et al.* [2008]: linear fit with different slope factors for two height intervals, thus assuming a slope for the height interval 12–24 m agl twice that of the slope observed in the layer 6–12 m agl. Horizontal interpolation was performed using the procedure described in section 4.3. Because the obtained 3-D wind fields were not mass conservative, we applied a correction for mass conservation according to the procedure described below (section 4.4).

4.4. Air Mass Conservation Correction

[54] Taking an integral of equation (11) over the control volume and then applying the Gauss theorem we obtain

$$\iint_S \overline{n}_{tot}\,\overline{\mathbf{u}} \cdot d\mathbf{S} = \Delta Q \tag{14}$$

where S is the surface of the control volume and ΔQ is the mass conservation deficit/excess. Positive values of ΔQ signify air transport out of the control volume, while negative ΔQ values refer to air flux into the control volume. The term $\overline{n}_{tot}\,\overline{\mathbf{u}} \cdot d\mathbf{S}$ for each elementary surface (named later elementary flux) is modified with a correction factor so that in the case of $\Delta Q < 0$ it implies the decrease of negative and the increase of positive elementary fluxes, and vice versa.

[55] Using the already calculated 3-D air density and wind velocity fields, the deviation ΔQ from the mass conservation was numerically estimated for each half-hour:

$$\Delta Q = \sum\nolimits_i \overline{n}_{tot_i}\,\overline{u}_i\,\Delta S_i \tag{15}$$

where ΔS_i are the 1 m^2 elementary surface elements of the control volume, $\overline{n}_{tot_i}$ is the average air density for each surface element and $\overline{u}_i$ is the average wind velocity component perpendicular to each surface element.

[56] In order to perform the numerical adjustment, a correction factor, *cf*, was defined. It is formed by the ratio of the mass conservation deficit/excess in the whole control volume, ΔQ, and the overall sum of the absolute values of the elementary fluxes:

$$cf = \frac{\Delta Q}{\sum_i \left|\overline{n}_{tot_i}\,\overline{u}_i\,\Delta S_i\right|} \tag{16}$$

and the following correction was performed:

$$\text{if } \overline{n}_{tot_i}\,\overline{u}_i\,\Delta S_i > 0 \text{ then } \overline{n}_{tot_i}\,\overline{u}_i\,\Delta S_i \rightarrow (1 - cf)\overline{n}_{tot_i}\,\overline{u}_i\,\Delta S_i$$
$$\text{if } \overline{n}_{tot_i}\,\overline{u}_i\,\Delta S_i < 0 \text{ then } \overline{n}_{tot_i}\,\overline{u}_i\,\Delta S_i \rightarrow (1 + cf)\overline{n}_{tot_i}\,\overline{u}_i\,\Delta S_i$$

This numerical correction guarantees mass conservation in the control volume, that is to say, ΔQ approximates zero. The corrected values for the product of air density and wind are then used to estimate the advective CO_2 fluxes on the surface of the control volume, equation (7).

[57] To assure coherence between term *II* and *III* of equation (6), we must assume that the $\overline{n}_{tot}$ 3-D field is not changed by *cf*. The corrected wind values ($\overline{\mathbf{u}}_{corr}$) assuring air mass conservation can be computed by the expression:

$$\overline{\mathbf{u}}_{corr} = \frac{(\overline{n}_{tot}\,\overline{\mathbf{u}})_{corr}}{\overline{n}_{tot_m}} \tag{17}$$

where $(\overline{n}_{tot}\,\overline{\mathbf{u}})_{corr}$ are values after application of the correction procedure and $\overline{n}_{tot_m}$ are values estimated from the measurements.

4.5. NEE Calculation

4.5.1. Advection Term (*Fca*)

[58] Here we will briefly outline only the framework of the method used for *Fca* computation, summarized in the Figure 3 flowchart.

[59] The application of the interpolation procedures described in the previous sections leads to a 3-D reconstruction of the physical quantities of interest in the control volume. Calculation of the advective flux, following equation (7), requires only the use of the respective quantities for

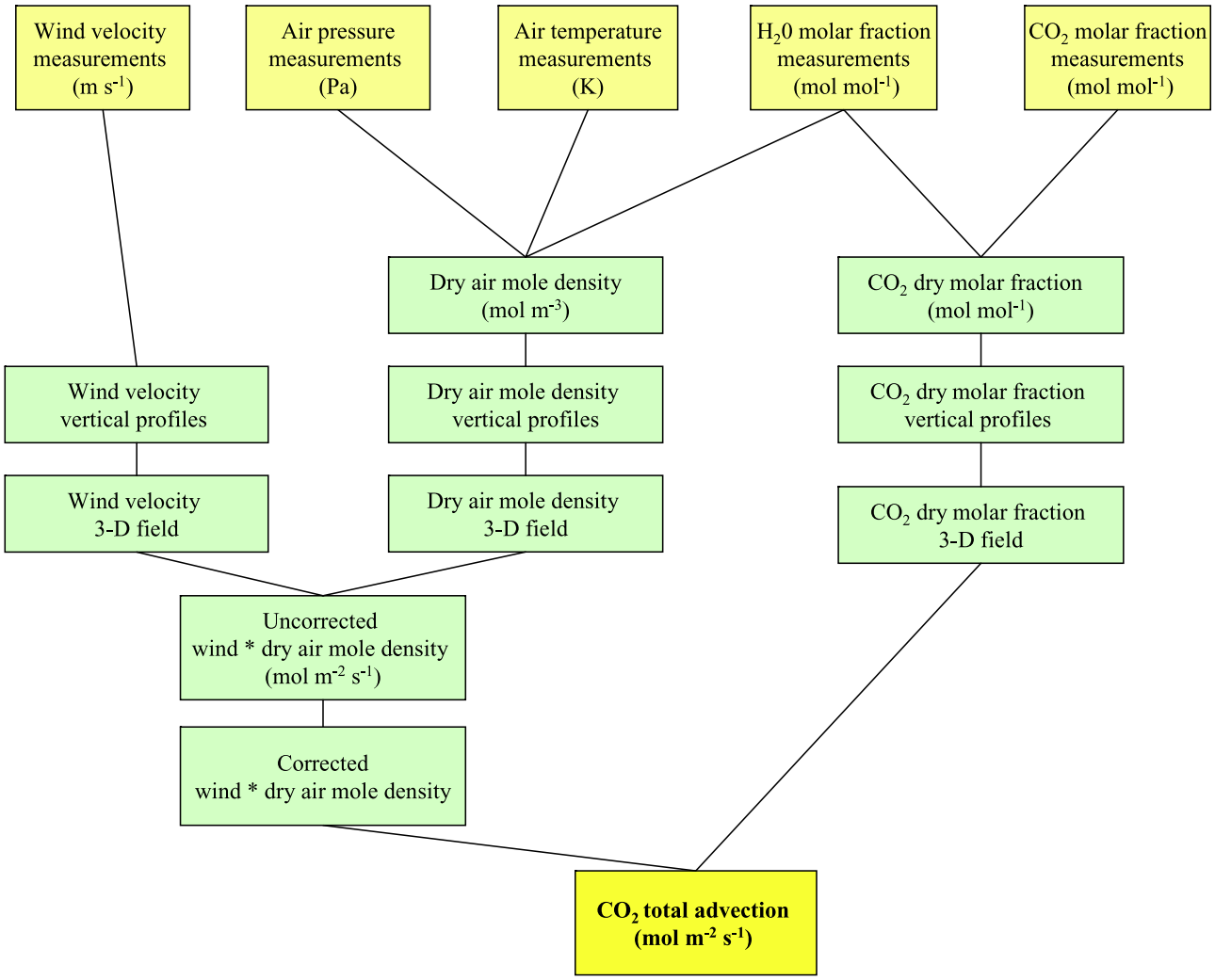

Figure 3. Flowchart of advection flux computation. In the upper line, input data are represented. All these data are georeferenced, and a digital elevation model of the terrain is requested as input. Algorithms used for interpolations, or to attain mass conservation, are described in section 4.

each volume cell (1 m^3) sited along each discrete surface element (**S**) of the control volume. Term *III* of equation (6) is approximated by the following equation:

$$\iint_S \overline{n}_c\,\overline{\mathbf{u}}\cdot d\mathbf{S} \approx \sum_j \overline{n}_{tot_j}\,\overline{u}_{corr_j}\,\overline{r}_{c_j}\,\Delta S_j \qquad (18)$$

According to the micrometeorological convention, a negative value is assigned to the fluxes entering the volume and a positive value is given to those leaving it.

[60] Summing the individual advective fluxes entering or exiting from the control volume boundary surfaces (Figure 4), a total advective flux relative to the entire control volume is obtained. In order to obtain the unitary advective flux, the total advective flux is divided by the area covered by the control volume.

4.5.2. Storage Term (*Fcs*)

[61] The storage term (*Fcs*) was calculated with the time resolution (30 min) widely used within the Fluxnet community, but the space resolution was adapted to the specific case study. *Fcs* was calculated by the equation:

$$\iiint_V \frac{\partial \overline{n}_c}{\partial t}\,dV \approx \sum_j \frac{\overline{n}_{tot_j(t+\Delta t)}\,\overline{r}_{c_j(t+\Delta t)} - \overline{n}_{tot_j(t)}\,\overline{r}_{c_j(t)}}{\Delta t}\,\Delta V_j \qquad (19)$$

where ΔV_j are the 1 m^3 elementary volume elements of the control volume, Δt is the 30-min averaging time interval, $\overline{n}_{tot_j}$ (μmol m^{-3}) is the average density of dry air for each volume element at time t or $t + \Delta t$ and $\overline{r}_{c_j}$ is the average CO_2 mole density (μmol mol^{-1}) for each volume element at time t or $t + \Delta t$. Similarly, this storage flux is normalized by the same reference surface used in advective flux computation. CO_2 storage is calculated using 30-min averaged molar density profiles, although errors due to fast variations in CO_2 density may be introduced [*Finnigan*, 2006]. The accuracy of calculations is also influenced by limited n_{tot} and r_c measurements: they were measured at the four external towers, but not at the central one.

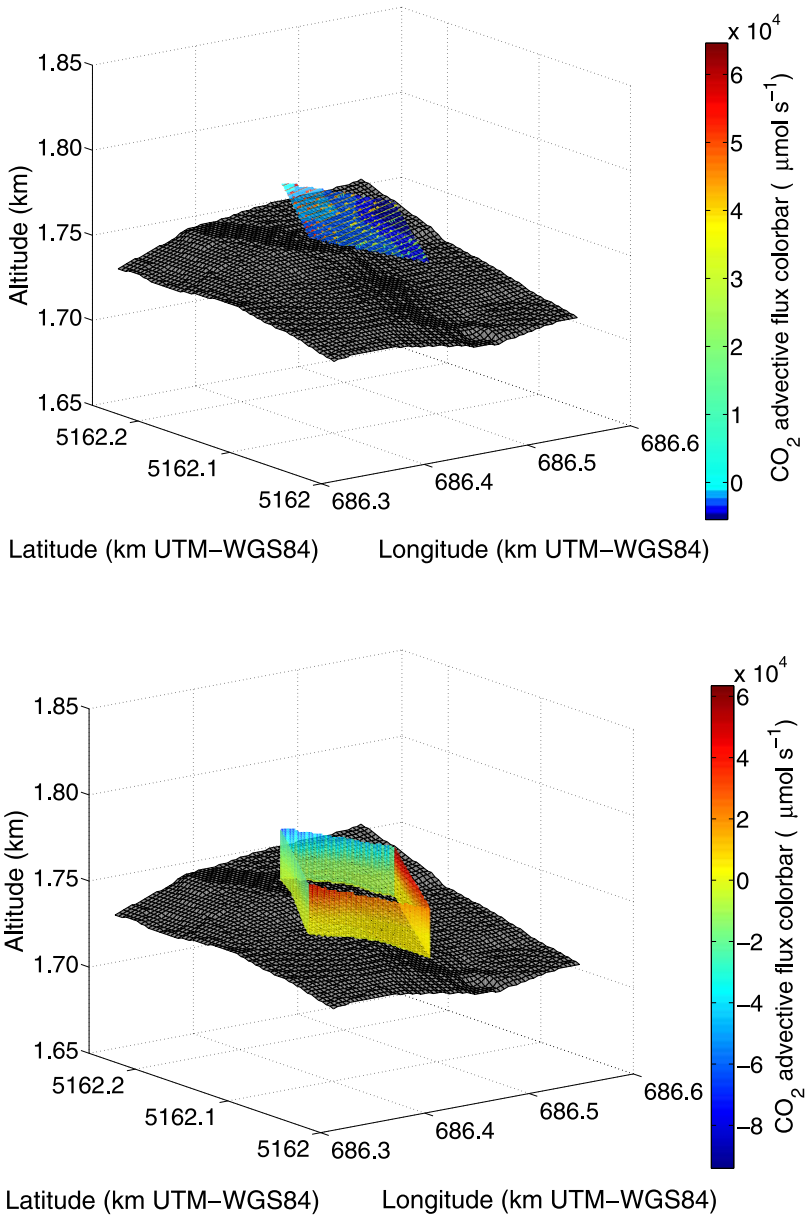

Figure 4. Example of advection flux calculated on the control volume top surface (top) and lateral surfaces (bottom). Blue (red) colors indicate negative (positive) advection; different scales are used to represent advection flux for lateral or top surfaces. Data refer to day 192 at 0000 LST.

[62] An additional source of uncertainty in *Fcs* computation is related to the fact that *Fca* and *Fct* data are estimated at time t, while *Fcs* is computed for the time interval between t and $t + \Delta t$.

4.5.3. Turbulent Transport Term (*Fct*)

[63] As a first approximation of term *IV* of equation (6), the long-term EC turbulent flux measured at central tower M was used, so *Fct* was approximated by

$$\overline{w'n_c'} \approx \iint_S \overline{n_c'\mathbf{u}'} \cdot d\mathbf{S} \tag{20}$$

We used a traditional approach for *Fct* computation. A two-axis rotation of coordinates [*McMillen*, 1988] was applied each half-hour, therefore term *IV* of equation (6) was approximated with the vertical turbulent flux in this rotated coordinate system, the horizontal turbulent flux divergence was neglected. Some authors point out its importance, e.g., *Moderow et al.* [2007] found that a noticeable heat divergence may be significant at night for a forest ecosystem; *Sun et al.* [2007] stressed that the horizontal divergence may be on the same order of magnitude as the vertical one. However, *Staebler and Fitzjarrald* [2004] reported results for horizontal eddy flux divergence to be usually no more than 10% of vertical flux, and less than 30% of mean advection. *Finnigan* [1999] argued that this term is probably small for a linear model of flow over a forested hill [*Raupach et al.*, 1992]. Noting that horizontal

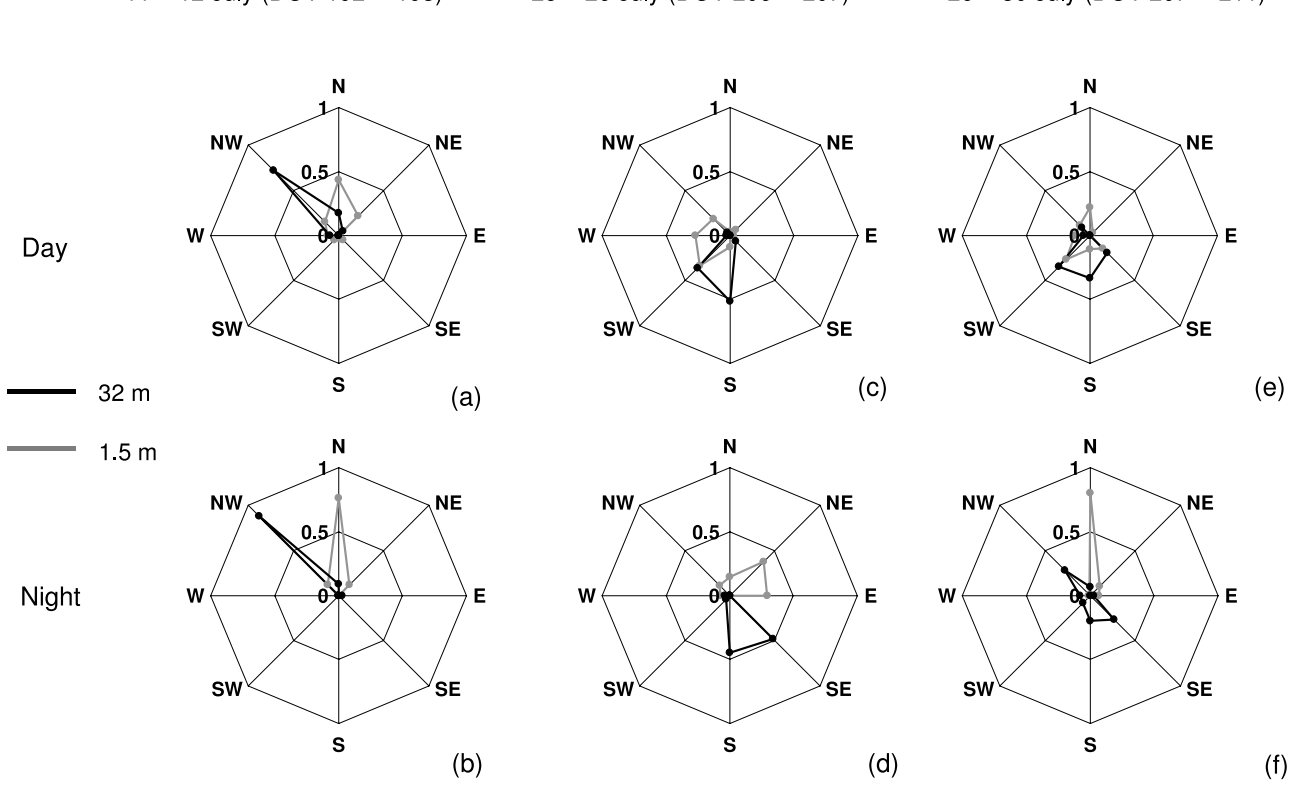

Figure 5. Frequencies of wind direction at tower M, measured during selected periods. Black line refers to above-canopy measurements (32 m); gray line refers to measurements taken at 1.5 m. Northerly winds, (a) day and (b) night. Southerly winds, (c) day and (d) night. Mountain valley wind system, (e) day and (f) night. Values refer to wind direction for each of the eight sectors 45° wide.

turbulent flux divergence requires further studies, we will neglect it in the present analysis.

5. Results and Discussion

5.1. Description of the Study Period

[64] The data set obtained during the month of July 2005 was selected for the analysis. This month was characterized by the highest values of incoming global radiation and air temperature in the measurements of the Advex campaign. Its choice was based on the presence of the three typical flow conditions mentioned in section 2 and it was when the instruments produced the highest percentage of unambiguously valid data (section 3).

[65] Three different time periods were considered in more detail. Taking as the reference the wind directions observed at 1.5 and 32 m agl (Figure 5) on the central tower M, each of these intervals represents one of the typical flow conditions described at the end of section 2:

[66] 1. A 48-h period characterized by synoptically driven strong northerly winds, locally called ''Tramontana'' (Figure 6a): from 0030 LST (Local Standard Time) of 11 July (day 192) to 2400 LST of 12 July (day 193). The sky was irregularly cloudy, net radiation was (mean ± SD) 450 ± 212 W m^{-2} during the day and −65 ± 20 W m^{-2} at night (Figure 6b);

[67] 2. A 30-h period characterized by southerly winds: from 0030 LST of 25 July (day 206) to 0600 LST of 26 July (day 207). The sky was overcast, net radiation was 368 ± 70 W m^{-2} during the day and −4 ± 5 W m^{-2} at night;

[68] 3. A 108-h period characterized by a local mountain valley wind system in the area, resulting in a below-canopy downslope (northerly) wind at night, and upslope (southerly) wind during the day: from 1200 LST of 26 July (day 207) to 2400 LST of 30 July (day 211). Fair weather conditions were present, net radiation was 666 ± 70 W m^{-2} during the day and −63 ± 33 W m^{-2} at night. During this period were observed the highest temperature and the highest temperature gradient within the canopy (Figure 6c).

[69] In this analysis the hours 0930–1500 LST are considered daytime, from 2130 to 0300 LST as nighttime, from 0530 to 0800 LST and from 1730 to 2000 LST as transitional hours.

5.2. Physical Quantities of Interest in the Control Volume

[70] We outline here the main characteristics of the observed variables relevant to the advection calculation, the so-called physical quantities of interest (section 4.2), during the selected time periods.

5.2.1. Total Mole Density of Dry Air (n_{tot})

[71] According to equation (12) the variability of temperature is an important factor in the variability of the total mole density of dry air. The first selected period was characterized by a positive thermal gradient during the night; the temperature difference in the layer between

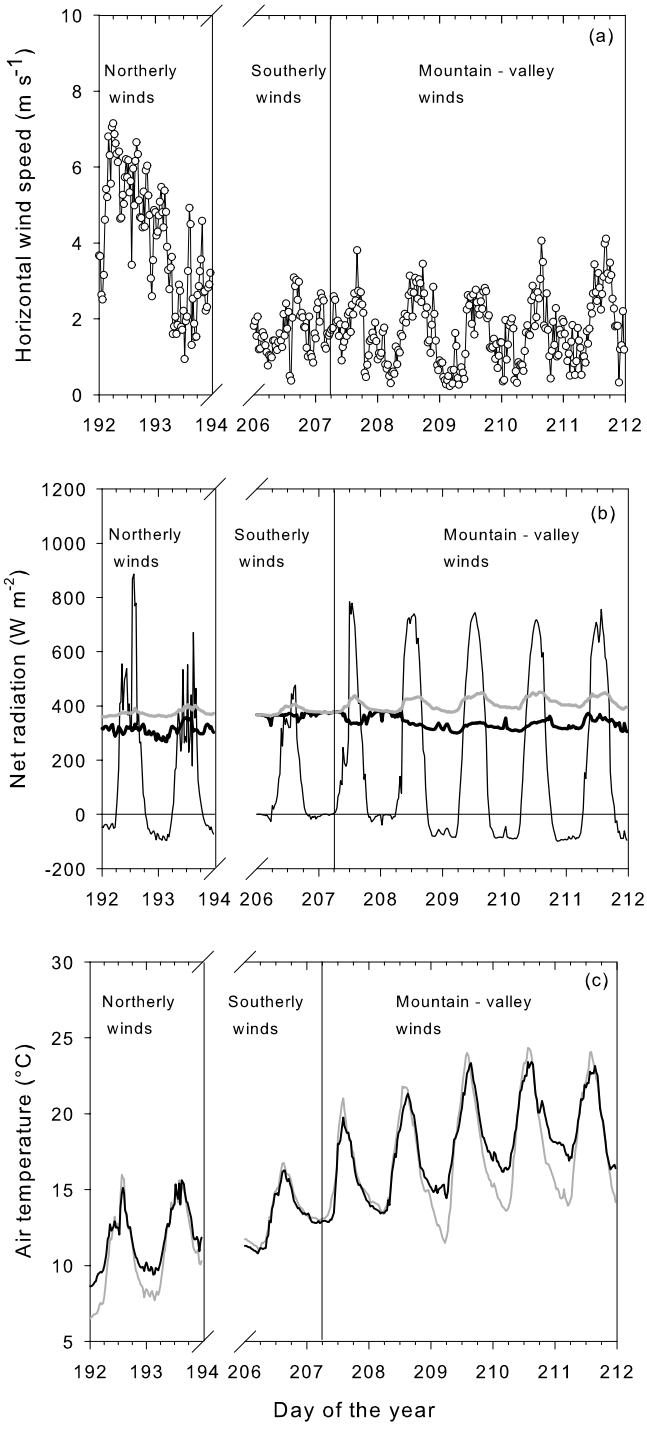

Figure 6. Meteorological parameters observed during selected periods. (a) Horizontal wind speed at 32 m agl, measured at tower M. (b) Radiation fluxes: net radiation (thin black line), longwave upward radiation (gray line), longwave downward radiation (solid black line). (c) Air temperature measured at 30 m on tower C (solid black line), 1.5 m on tower C (gray line). Data refer to the period 11–12 July (day 192–193) and to the period 25–30 July (day 206–211).

30 m and 1.5 m was positive at all towers, with a mean value of 1.34°C. The highest value of total mole density of dry air $\overline{n}_{tot}$, 35.03 mol m^{-3} was estimated at the lowest measuring point in the control volume (1.5 m agl tower C), while the lowest value, 34.63 mol m^{-3}, was calculated at the highest measuring point, 30 m agl at tower A. The vertical profile, similar at all towers, showed values that decreased with height. During the central hours of the day the temperature gradient in the layer 30–1.5 m agl was negative, with an average value for all towers of about −0.9°C. Total mole density of dry air $\overline{n}_{tot}$ was quite similar at all measurement points, in the range from 34.17 to 34.26 mol m^{-3}, but observed $\overline{n}_{tot}$ values exhibited various profiles at the different towers, which were also related to the presence of a recirculation zone under the canopy during the day.

[72] In the second period, when winds from the south prevailed, the temperatures during the nights were 2–4°C higher than in the case of the northern Tramontana. The observed values of $\overline{n}_{tot}$ (range between 33.94 and 34.11 mol m^{-3}) were lower than those in the first period. Maximal $\overline{n}_{tot}$ values were observed near the ground, both night and day.

[73] For the third case, mountain valley wind circulation, the temperatures both during day and night were the highest among the selected time periods, e.g., daytime temperatures under the canopy reached approximately 21°C. The nighttime inversion, with a mean temperature difference of 1.6°C between 30 and 1.5 m was stronger than in the case of the Tramontana. As a consequence, the vertical variability of $\overline{n}_{tot}$ was also noteworthy: peak values were observed near the ground, smallest at 30 m agl. The range was from 34.06 mol m^{-3} (observed at the lowest measuring point in the control volume, 1.5 m agl at tower C) to 33.66 mol m^{-3} (observed at the highest measuring point in the control volume, 30 m agl at tower A). During the day, under unstable conditions, higher values of $\overline{n}_{tot}$ were observed not near the ground, but mainly at 30 m agl.

5.2.2. CO_2 Dry Molar Fraction (r_c)

[74] The shape of the half-hour averaged vertical profiles of the CO_2 dry molar fraction, $\overline{r}_c$, during the night was typically an exponential function of height, as demonstrated in Figure 7a using data from the third selected period. This type of profile was also observed for the transition hours, while for the daytime the profile was almost straight, with a poorly defined minimum of $\overline{r}_c$ values in the canopy air layer due to photosynthesis. Vertical profiles of $\overline{r}_c$, averaged for all hours of the day, demonstrate that the highest values were measured close to the Earth's surface, as also shown by *Aubinet et al.* [2005].

[75] The differences in measured $\overline{r}_c$ values between the towers depended on the time of day, measurement height and the particular flow condition. Maximal $\overline{r}_c$ differences were observed during the night, close to the Earth's surface and for the period marked as mountain valley circulation. For example, the difference in $\overline{r}_c$ between towers C and D at level 1.5 m agl averaged for the night between days 210 and 211 was 30.5 μmol mol^{-1}, approximately twice the value measured during the same hours in the case of northern or southern winds. The differences in $\overline{r}_c$ between the towers tended to disappear with height and approach zero values at 30 m agl.

[76] During the day the differences in $\overline{r}_c$ between the towers were much smaller, e.g., about 3–4 μmol mol^{-1} at

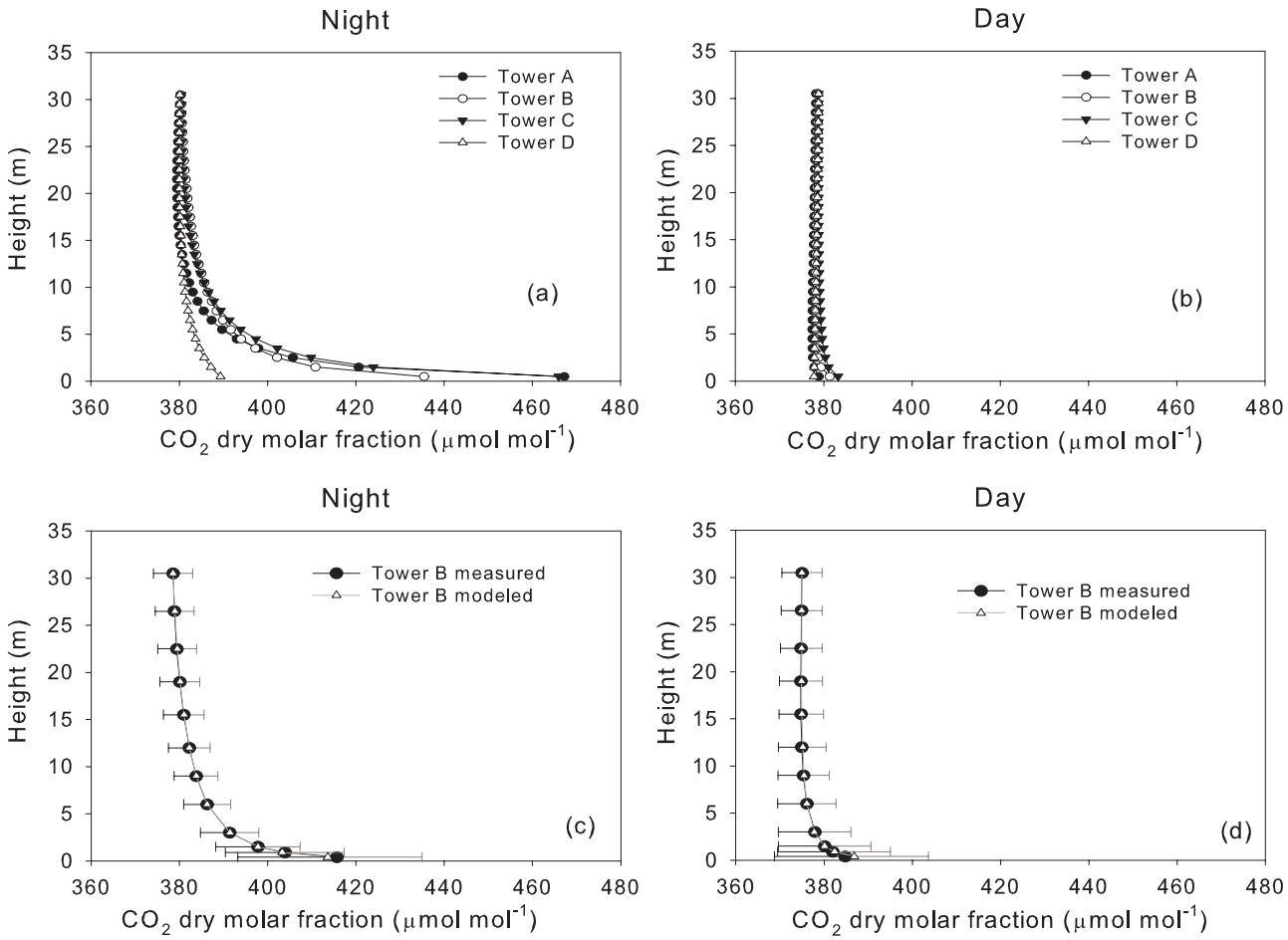

Figure 7. Average CO_2 dry molar fraction ($\bar{r}_c$, μmol mol^{-1}) during the mountain valley wind system period (day 207–211) modeled from data collected by the main sampling system at tower A, B, C, and D for (a) night and (b) day. CO_2 dry molar fraction measured and modeled at tower B by an independent system during the whole month of July at (c) night and at (d) day; gray error bars refer to +standard deviation (modeled data), and black bars refer to −standard deviation (measured data). Night refers to 2130–0300 LST, and day refers to 0930–1500 LST.

1.5 m agl between towers C and D (Figure 7b). Persistent maximal values were measured at tower C in the lowest part of the canopy air layer while minimal values were recorded in the middle part of this layer, similar to observations in a Siberian forest presented by *Styles et al.* [2002]. At the same time, minimal values of about 377.8 μmol mol^{-1} were observed at the lowest measurement level at tower D.

[77] In order to test the interpolation procedure for calculation of the $\bar{r}_c$ vertical profile in the canopy layer (section 4.3.2) the additional measurements at tower B (12 levels) were used. The values of the CO_2 dry molar fraction, measured at the main levels at tower B (1.5 m, 6 m and 30 m agl) were interpolated at the remaining nine levels: 0.4, 0.9, 3, 9, 12, 15.5, 19, 22.5 and 26.5 m agl. These modeled $\bar{r}_c$ values were compared to the measured values at the nine levels for the whole month of July 2005 (Figures 7c and 7d). The mean correlation coefficient between measured and modeled $\bar{r}_c$ values, taking into account all data from July 2005, was 0.972. The correlation coefficient varied with the hours of the day: the highest values were obtained during the night hours and the lowest values during the day hours. It is to be noted that through the interpolation by equation (13) it was not possible to calculate the secondary minimum of $\bar{r}_c$ occasionally observed at 0.4 m agl during the day, a value that reflects photosynthesis of the ground vegetation at this sampling point.

5.2.3. Wind Field

[78] The flow field in the control volume was quite different for the selected periods, as it was the result of the interaction of various factors: climate conditions, topography, heterogeneity of the canopy and variability of leaf area density (LAD).

[79] During northerly wind conditions the airflow entered the control volume after passing through uphill sectors with sparse trees and pastures. Thus, there was an abrupt increase in surface roughness a few meters before the control volume. During the night (Figure 8a) strong winds were present at 30 m agl at tower A, while lower wind velocities were observed downslope. During the day (Figure 8b) even higher velocities were observed above the canopy at tower A, with a similar reduction of wind velocity at tower C. Wind measurements at lower heights suggest the creation of a recirculation zone in the canopy; the horizontal wind vector at heights 1.5, 6 and 12 m agl at the downwind

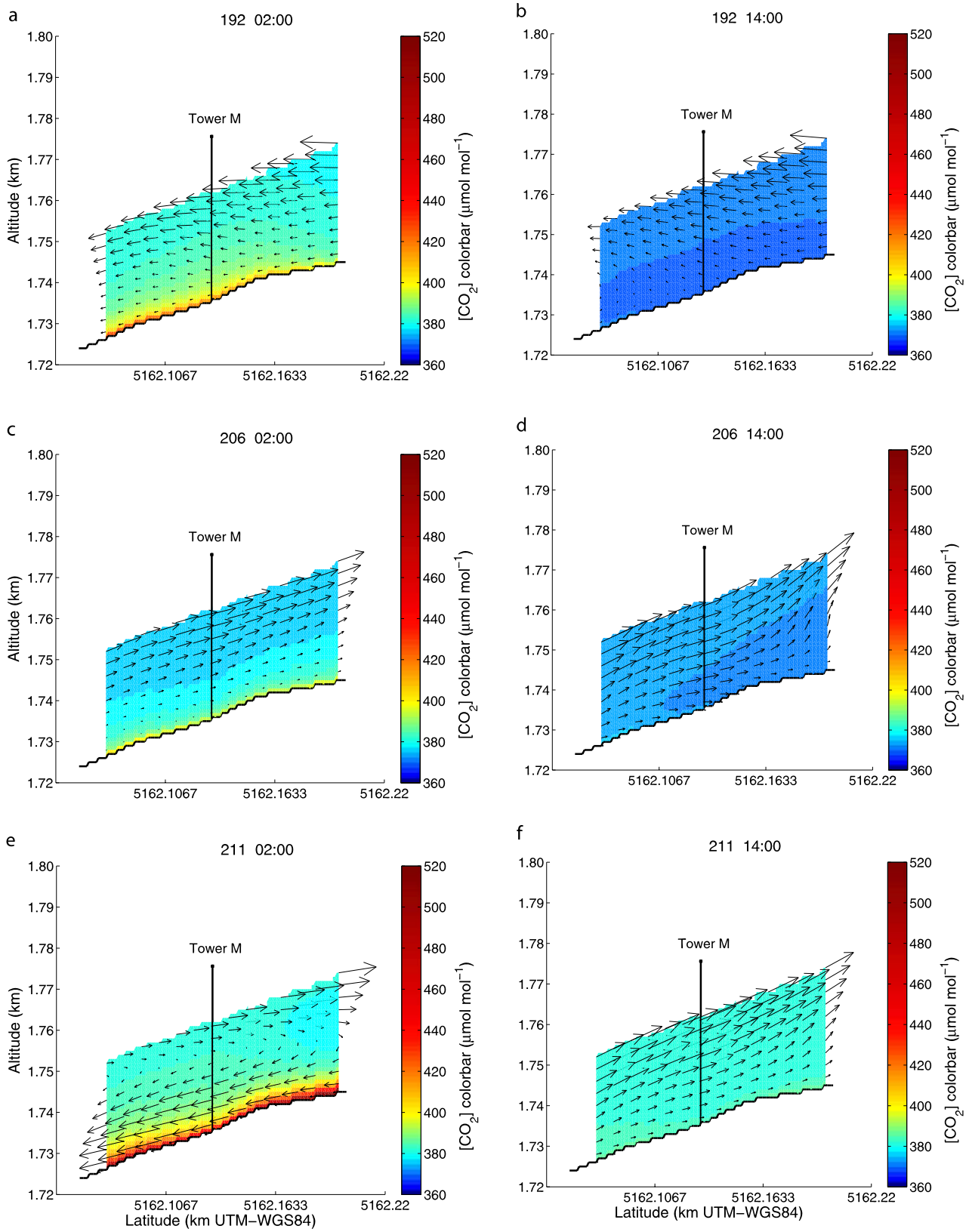

Figure 8. Wind and CO_2 dry molar fraction fields in N–S cross-sections for the selected periods. Northerly wind conditions, day 192, respectively for (a) 0200 LST and (b) 1400 LST. Southerly wind conditions, day 206, respectively for (c) 0200 LST and (d) 1400 LST. Mountain valley wind system, day 211, respectively for (e) 0200 LST and (f) 1400 LST. Notice different scales for the arrows: maximum arrow size is (Figure 8a) 3.3 m s^{-1}, (Figure 8b) 4.2 m s^{-1}, (Figure 8c) 1.0 m s^{-1}, (Figure 8d) 0.7 m s^{-1}, (Figure 8e) 0.9 m s^{-1}, and (Figure 8f) 1.9 m s^{-1}.

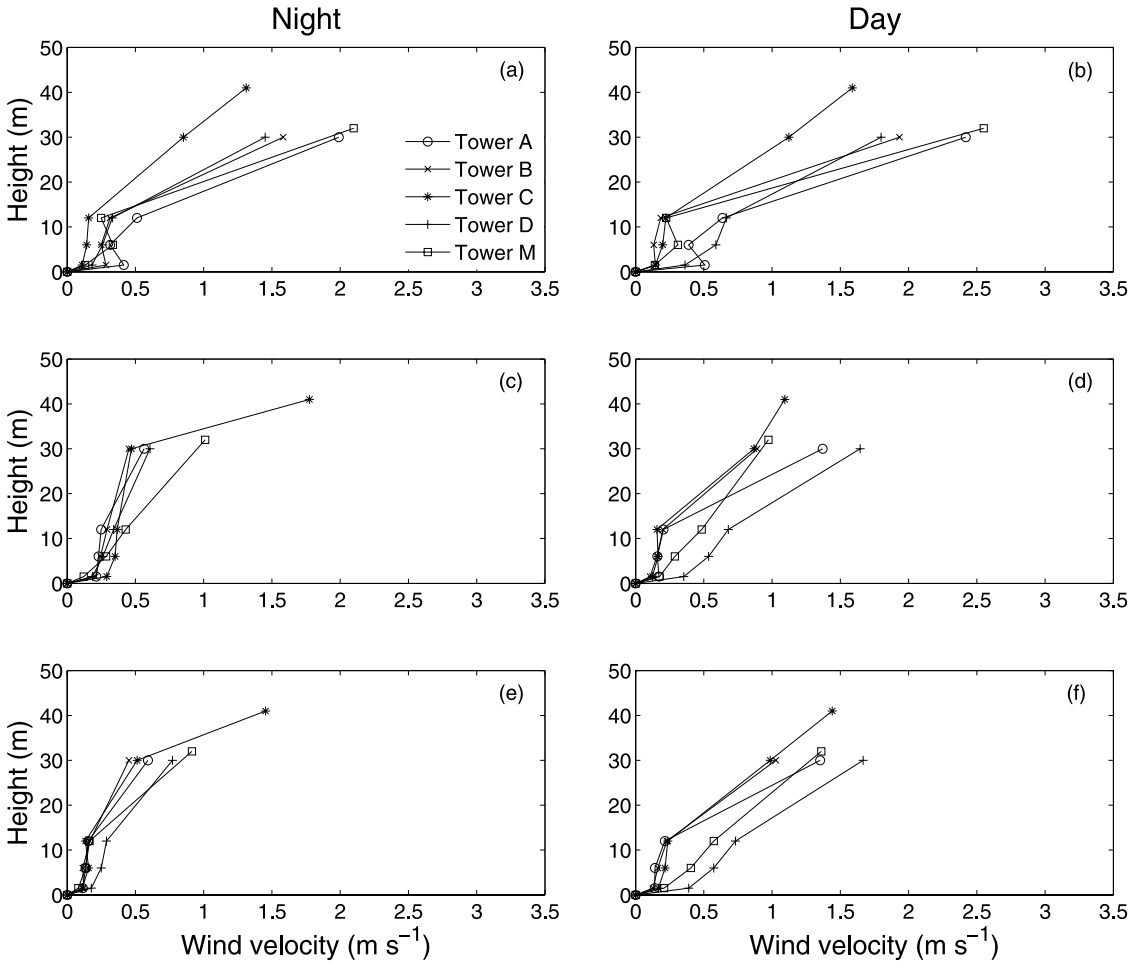

Figure 9. Profiles of the $\overline{\mathbf{u}}$ module at towers A, B, C, D, and M. Night and day mean values during selected periods. (a, b) Northerly winds; (c, d) southerly winds; (e, f) mountain valley wind system.

towers B and C were directed upslope and thus were opposite to the direction of the wind above the canopy. This reverse wind, enhanced by buoyancy, is in accordance with recent analytical and numerical results [*Finnigan and Belcher*, 2004; *Katul et al.*, 2006; *Poggi and Katul*, 2007] for the flow above dense canopies on gentle hills. During north wind conditions wind speed profiles were not linear, with an S-shaped profile within the canopy at the towers where an open trunk space was present (Figures 9a and 9b).

[80] In southerly wind conditions (Figures 8c and 8d) winds from the south encountered a homogeneous mature forest along its path length. In the control volume, winds encountered an irregular canopy with a dense understory. Wind velocity above the canopy increased from the southern tower (C) to the northern tower by 30% during the night and by 57% during the day. These higher values at the downwind tower may be explained by two main factors: effects of the orography outside the control volume and lower canopy height with respect to the conditions at the impact with tower C. Under the canopy the flow was affected by the dense understory and a decrease in wind speed by a similar percentage was observed. Vertical wind profiles were almost linear at all the towers between 6 and 30 m agl at night (Figure 9c) and assumed different shapes during the day (Figure 9d).

[81] The thermally induced mountain valley wind circulation occurred in about 75% of the summer period. This circulation was well expressed in the observations: downslope (northerly) winds during the night, upslope (southerly) winds during the day and their alternation during the transition phases in the evening and in the morning. The evening transition began well before sunset, at around 1800 LST. During this transition the winds changed from upslope to downslope. The opposite was observed in the morning, when anabatic winds, measured initially above the canopy, gradually prevailed over downslope northerly winds. During the night, a downslope wind developed in a shallow layer over the ground while above this layer the wind was in the opposite direction (Figure 8e). The decoupling between above- and below-canopy flows persisted during all nights of the period except for a few half-hour intervals between day 208 and 210, when downslope flow was detected even at the highest measurement point (41.5 m agl at tower C). The speed of the downslope wind, its acceleration along the main slope, as well as the thickness of its layer, depended on various factors: the distance from the hill crest, the Richardson number of the flow, the slope of the terrain and the net radiation [e.g., *Whiteman*, 2000; *Mahrt et al.*, 2001; *Princevac et al.*, 2005]. In average, at night the wind velocity profiles had similar values at all towers, with an

Table 2. Mass Variation in the Control Volume and Correction Factor Calculated During Three Periods Selected for Winds Conditions and During the Whole Month of July[a]

		ΔQ		cf	
		Average	SD	Average	SD
	n	(mol dry air m^{-2} s^{-1})	(mol dry air m^{-2} s^{-1})	(Adimensional)	(Adimensional)
Northerly wind night	24	2.65	0.77	0.040	0.018
Northerly wind day	23	1.00	1.90	0.004	0.031
Southerly wind night	18	−1.99	1.57	−0.065	0.044
Southerly wind day	9	−2.63	1.01	−0.075	0.025
Mountain valley wind system night	53	0.27	1.57	0.017	0.072
Mountain valley wind system day	52	−3.39	1.24	−0.072	0.030
July night	318	1.50	1.95	0.036	0.062
July day	292	−2.00	1.95	−0.056	0.046
Northerly wind night (*Fct* QA)	23	2.65	0.77	0.040	0.018
Northerly wind day (*Fct* QA)	20	1.11	1.95	0.005	0.033
Southerly wind night (*Fct* QA)	10	−1.97	0.93	−0.070	0.013
Southerly wind day (*Fct* QA)	4	−3.28	1.00	−0.088	0.018
Mountain valley wind system night (*Fct* QA)	24	−0.14	1.53	−0.005	0.055
Mountain-valley wind system day (*Fct* QA)	41	−3.46	1.22	−0.072	0.028
July night (*Fct* QA)	185	1.85	2.06	0.030	0.052
July day (*Fct* QA)	224	−2.12	2.09	−0.058	0.047

[a]*Fct* QA refers to data collected when turbulent flux passed the quality test for stationarity and integral turbulent characteristics. Mass variation in the control volume, ΔQ; correction factor, *cf*.

almost logarithmic shape in the canopy air space (Figure 9e). The S-shaped vertical profile, typical of forests with an open trunk space [*Yi et al.*, 2005] was observed only occasionally at towers B and C. Profiles of the single wind components (u, v, w) frequently showed both negative and positive values with height, due to the decoupled flow below and above the canopy.

[82] During the day, upslope winds were observed at all towers without decoupling of the flow below and above the canopy (Figure 8f). The direction of the upslope wind was southeasterly (prevailing at all levels of towers D and M), or southwesterly, observed usually under the canopy at towers A, B and C, reflecting the influence of the two adjacent Isarco and Sarentino valleys. The shape of the vertical profiles was almost linear, but variable from site to site (Figure 9f).

[83] Under such conditions of strong spatial and temporal variability of the wind components, uncertainties may arise from the use of a single interpolation technique. In the case of a logarithmic profile, the applied vertical linear interpolation probably overestimates wind velocity in the height interval from 12 to 30 m agl. The vertical profile proposed by *Feigenwinter et al.* [2008] is a good approximation for the logarithmic type of profile, but wind velocity values in this height interval are underestimated for an S-shaped profile, while those for a linear type are overestimated. Later, in section 5.3, it will be shown that the type of vertical interpolation has a significant effect on ΔQ.

5.3. Air Mass Conservation Correction

[84] The air mass conservation procedure involves interpolated half-hourly values of $\overline{n}_{tot}$ and the wind components. Averaged values of air temperature, air pressure and water vapor mole density may change from one half-hour to the next. These variations, which normally give a nighttime maximum and a daytime minimum in n_{tot}, were accounted for before imposing air mass conservation.

[85] However, because of experimental limits and uncertainties in interpolations, the air mass balance calculated along the surface of the control volume was seldom close to zero. The observed ΔQ was strongly dependent on the wind regime, on the time of the day and on the interpolation method, particularly on the vertical interpolation of the wind components. Furthermore, it changed in relation to stationarity or ITC conditions (Table 2). These differences in ΔQ affect the magnitude of the correction factor *cf*.

[86] ΔQ and *cf* were found to be generally positive in conditions of northerly winds, and negative for southerly winds. During the month of July mean values of ΔQ were positive during the night (mean ± SD, 1.50 ± 1.95 mol m^{-2} s^{-1}) and negative during the day (−2.00 ± 1.95 mol m^{-2} s^{-1}). Averaged values of *cf* were also positive at night and negative during the day, being 0.036 ± 0.062 and −0.056 ± 0.046 respectively. Using the vertical interpolation proposed by [*Feigenwinter et al.*, 2008], ΔQ values were lower during the night (1.37 ± 1.72 mol m^{-2} s^{-1}) but showed larger negative values during the day (−2.21 ± 1.69 mol m^{-2} s^{-1}).

[87] For the three selected periods, the highest positive values of ΔQ were found during the Tramontana nights, while the largest negative values were found during the day in the period of mountain valley wind (see Table 2). The highest positive values of *cf* were also obtained during Tramontana nights, while the highest negative values were found for southerly winds during the day. It must be stressed, however, that the highest absolute values of *cf*, up to 0.25, resulted for stable nighttime hours during the mountain valley wind system (Figure 10a), in conditions when the ITC test for turbulent flux quality was not passed and the Richardson number, calculated at tower B for the height interval from 1.5 m to 30 m agl, was above 1.

5.4. CO_2 Fluxes

[88] An overview of the calculated CO_2 fluxes for the different flow conditions is given in Table 3. In the following sections the fluxes are discussed in details, outlining their relative uncertainties as well.

5.4.1. CO_2 Advective Flux (*Fca*)

[89] The estimated advective flux turned out to be the NEE component most influenced by the different flow

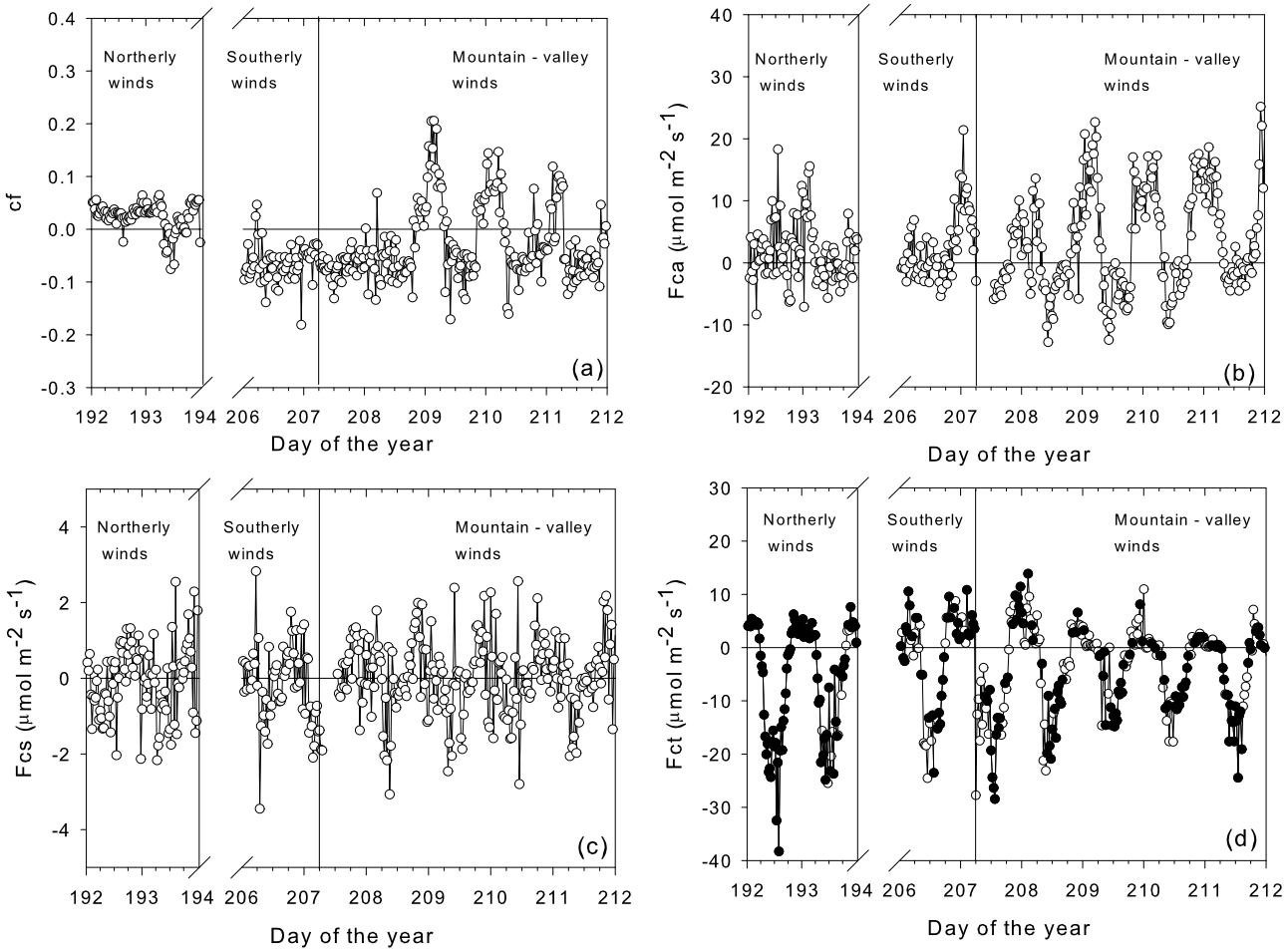

Figure 10. Correction factor and measured CO_2 fluxes during selected periods. (a) Correction factor (*cf*); (b) advection flux (*Fca*); (c) storage flux (*Fcs*); (d) turbulent flux (*Fct*). Black symbols refer to values that passed the quality test for stationarity and Integral Turbulent Characteristic (ITC).

conditions. Thus, its contribution to the NEE was also variable, being either negligible, or representing the largest part of it.

[90] 1. Northerly wind conditions: The total CO_2 advective flux was prevailingly positive during the first 30 h of the period, both by night and day, while during the daytime on day 193 (0600–2000 LST) it was prevalently negative, -0.7 ± 2.8 μmol m^{-2} s^{-1} (Figure 10b). The mean nighttime advective flux was 3.7 ± 6.0 μmol m^{-2} s^{-1}.

[91] 2. Southerly wind conditions: During the first part of the period the total advective flux oscillated around zero (mean value 0.4 ± 2.7 μmol m^{-2} s^{-1}) for the daytime hours, while during the night it was weakly positive (mean value 3.3 ± 5.3 μmol m^{-2} s^{-1}). This pattern changed at the beginning of day 207 because of the changed flow conditions. While the wind above the canopy maintained the northward direction, a southwesterly flow developed under the canopy (similar to the third selected period, characterized by southwesterly slope winds). There was an enhanced advection with mean flux of 12.6 ± 4.7 μmol m^{-2} s^{-1}.

[92] 3. Mountain valley wind system: During the night, in the presence of downslope winds, both n_{tot} and r_c increased along the below-canopy wind direction, leading to significant positive advection (Table 3 and Figure 10b). *Fca* was 10.8 ± 6.1 μmol m^{-2} s^{-1}, representing the main part of the total ecosystem respiration, 76.9% on the average. The highest values of *Fca* were calculated for the time intervals when the Richardson number, estimated for the layer from 1.5 to 30 m agl at tower B, was greater than 1 (Figure 11). During the transition hours, advective flux values were on average positive but highly variable. The evening transition from negative to positive values was generally found at 1900–1930 LST, 1 hour before sunset. The morning transition from positive to negative advective values was generally intermittent and took place in the time interval 0600–0800 LST, about 1 to 3 h after sunrise, when a fully developed upslope wind was present.

[93] During the day the advective flux showed negative values before noon, but values close to zero at the beginning of the afternoon (1300 LST). This decrease in negative advection was not associated with significant variations in friction velocity or wind direction, but with lower r_c gradients below the canopy. In the late afternoon (1400–1800 LST) the total advective flux was slightly negative, with low variability. The total advective flux, averaged on the daylight period (0530–2000 LST), was close to zero (-0.9 ± 6.0 μmol m^{-2} s^{-1}), but if we exclude the morning and evening transition hours we obtain a significant nega-

Table 3. CO_2 Fluxes Calculated During Three Periods Selected for Wind Conditions and During the Whole Month of July

		Fca		*Fcs*		*Fct*		NEEa		NEEb	
		Average	SD	Average	SD	Average	SD	Average	SD	Average	SD
	n	(μmol CO_2 m^{-2} s^{-1})	(μmol CO_2 m^{-2} s^{-1})	(μmol CO_2 m^{-2} s^{-1})	(μmol CO_2 m^{-2} s^{-1})	(μmol CO_2 m^{-2} s^{-1})	(μmol CO_2 m^{-2} s^{-1})	(μmol CO_2 m^{-2} s^{-1})	(μmol CO_2 m^{-2} s^{-1})	(μmol CO_2 m^{-2} s^{-1})	(μmol CO_2 m^{-2} s^{-1})
Northerly wind night	24	3.73	6.01	0.02	1.03	3.96	1.39	3.98	1.56	7.71	5.17
Northerly wind day	23	2.53	5.29	−0.26	1.11	−19.73	7.13	−19.99	7.68	−17.46	5.86
Southerly wind night	18	6.45	4.42	−0.03	0.22	3.21	14.68	3.18	14.91	9.63	19.33
Southerly wind day	9	0.19	2.45	−0.34	0.79	−17.56	4.25	−17.90	4.39	−17.71	5.33
Mountain valley wind system night	53	10.81	6.13	0.20	0.94	3.16	3.57	3.35	3.69	14.17	5.40
Mountain valley wind system day	52	−4.55	3.55	−0.23	0.83	−13.43	5.27	−13.66	5.46	−18.21	6.02
July night	318	8.88	7.79	0.08	0.91	2.30	2.85	2.38	3.00	11.26	6.93
July day	292	−1.34	3.65	−0.24	0.74	−15.00	6.79	−15.24	6.97	−16.58	6.76
Northerly wind night (*Fct* QA)	23	3.19	3.36	−0.06	0.99	4.21	1.23	4.14	1.56	7.34	4.83
Northerly wind day (*Fct* QA)	20	2.94	4.90	−0.34	1.06	−20.34	7.40	−20.67	7.98	−17.74	6.04
Southerly wind night (*Fct* QA)	10	4.78	3.56	0.17	0.40	2.87	11.67	3.04	12.07	7.82	15.63
Southerly wind day (*Fct* QA)	4	−0.26	2.87	−0.39	0.82	−13.63	7.56	−14.03	6.89	−14.28	6.69
Mountain-valley wind system night (*Fct* QA)	24	9.14	4.90	0.30	0.85	4.59	3.78	4.89	3.74	14.03	3.89
Mountain-valley wind system day (*Fct* QA)	41	−3.82	3.36	−0.31	0.64	−13.95	4.92	−14.26	4.95	−18.08	5.85
July night (*Fct* QA)	185	6.52	7.45	0.16	0.97	3.22	2.48	3.38	2.64	9.90	6.68
July day (*Fct* QA)	224	−1.34	3.68	−0.24	0.71	−14.79	6.44	−15.02	6.63	−16.36	6.62

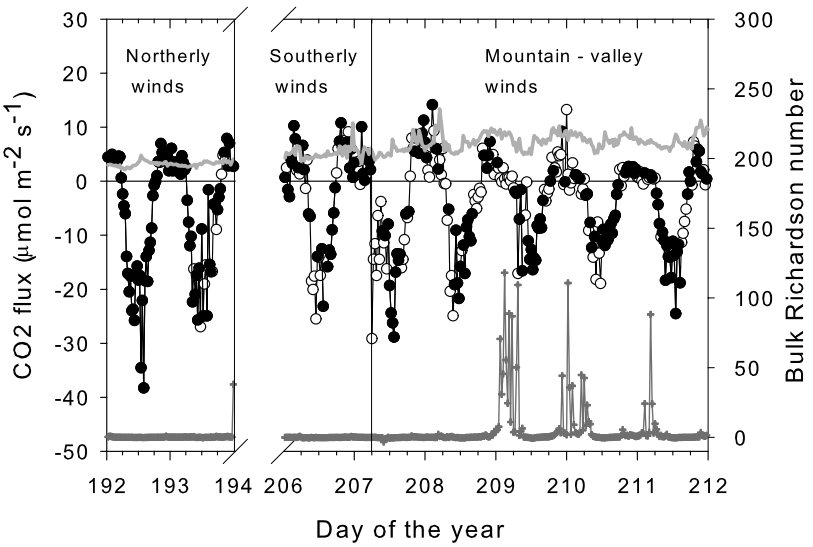

Figure 11. Sum of turbulent and storage fluxes (NEEa, black) and CO_2 efflux from the soil (light gray) measured by Li 8100-101 (primary *y* axis); Bulk Richardson number measured between 1.5 and 30 m at tower B (dark gray line, secondary *y* axis). Black symbols refer to values measured when *Fct* passed the quality test for stationarity and ITC.

tive value (-3.8 ± 3.7 μmol m^{-2} s^{-1} between 0830 and 1730 LST). The daytime negative advection, obtained only in upslope wind conditions, can be explained by horizontal r_c gradients existing inside the canopy. At the southernmost tower C, where the tree canopy was dense and continuous, a maximum of r_c near the ground persisted for most of the day. This was not the case for the more open forest growing upslope near towers A, D and M, where during the day a secondary minimum of r_c, related to understory photosynthesis, developed near the ground.

[94] The uncertainty related to advective flux computation depends on the following main factors: (1) accuracy and precision in the measurements of the input parameters for its calculation (wind direction and speed, air temperature, air pressure, CO_2 and H_2O mole densities); (2) number and spatial distribution of sampling points; (3) interpolation functions for obtaining the 3-D wind field; (4) the correction procedure used to attain air mass conservation.

[95] The correction factor (*cf*) applied in order to assure mass conservation depends on items (1)–(3) and determines the last one, (4) so it can be used as a synthetic indicator of calculated $\overline{\mathbf{u}}\,\overline{n}_{tot}$ uncertainty. Higher values of $|cf|$ indicate that air mass conservation is more violated.

[96] For *Fca* calculation it is necessary to multiply the mass conservative term $(\overline{\mathbf{u}}\,\overline{n}_{tot})_{corr}$ by the 3-D $\overline{r}_c$ scalar field computed on the surface of the control volume. The product $Fca = (\overline{\mathbf{u}}\,\overline{n}_{tot})_{corr}\ \overline{r}_c$ is affected by an error ε that can be estimated following the formula of error propagation in the product of independent variables, as

$$Fca + \varepsilon = (\overline{\mathbf{u}}\,\overline{n}_{tot})_{corr} + \eta + \overline{r}_c + \mu + \eta\,\mu \qquad (21)$$

where η and μ are errors in $(\overline{\mathbf{u}}\,\overline{n}_{tot})_{corr}$ and $\overline{r}_c$ respectively. The error ε affecting *Fca* can be computed on the basis of probability density functions of η and μ.

[97] To get an idea of the impact of η on *Fca* computation, we eliminated the data collected when *cf* was above a defined threshold. The correction factor *cf*, estimated on the basis of observed air density and wind data in the complex topography of Renon, showed maximum values of 0.25, ($|cf| \leq 0.25$). We defined as more reliable the data having $|cf| \leq 0.1$ and we flagged data with $|cf| > 0.1$, which were 10.8% of all the July data. The elimination of data with $|cf| > 0.1$ led to a 3.5% decrease in the mean nighttime (2130–0300 LST) value of *Fca*, while the mean daytime (0930–1500 LST) value of *Fca* remained unchanged. A similar statistical analysis was performed to study the impact of μ on *Fca*. By excluding the values when the R^2 between measured and modeled $\overline{r}_c$ values at tower B was below 0.9, we found that night values of Fca remained unchanged (R^2 never dropped below the threshold), while averaged day values of *Fca* were more negative (-2.4 μmol m^{-2} s^{-1} instead of -1.3 μmol m^{-2} s^{-1}).

[98] Additional uncertainty in *Fca* computation is given by the presence of nonsteady components of the flow, which can be significant particularly at dawn and at dusk, when rapid changes in temperature occur.

[99] The approach to *Fca* computation on the surface of the control volume is necessarily linked to the mass conservation principle. This bond is highlighted by the estimated ΔQ values, rarely close to zero because of the challenging conditions of this case study. To understand the importance of the air mass conservation correction in *Fca* computation we computed the *Fca* also without using the mass conservation correction. Because of fictitious inflow and outflow of air mass containing CO_2 (see Table 2), calculated *Fca* values were very large, being on the average 723 ± 741 μmol m^{-2} s^{-1} during the night (2130–0300 LST) and -772 ± 731 μmol m^{-2} s^{-1} during the day (0930–1500 LST), thus presenting values of 2 orders of magnitude greater than the *Fca* calculated by the method we propose.

5.4.2. CO_2 Storage Flux (*Fcs*)

[100] Storage flux was characterized by the lowest daily variability during the three selected periods (Figure 10c).

For all flow conditions *Fcs* showed prevailing positive values at sunset and negative values at sunrise, thus confirming the pattern revealed by *Marcolla et al.* [2005] and by *Aubinet et al.* [2005]. Compared to the other fluxes, storage flux was smaller: half-hourly averaged values were in the range between -4 and 4 μmol m^{-2} s^{-1}.

[101] Storage flux, calculated in our 3-D approach (equation (19)) showed values close to the averaged storage flux estimated traditionally on the basis of single tower measurements [*Baldocchi et al.*, 1988; *Aubinet et al.*, 2000]. Moreover, the values we obtained had a more regular daily pattern, being less sensitive to single CO_2 gusts than single tower estimates.

[102] Uncertainty in estimating storage flux appears to be related to the choice of the measurement site as well as to measurement and calculation methods and time averaging [*Finnigan*, 2006; *Yang et al.*, 2007]. To investigate the relationship between *Fcs* calculated from the four profiles (x) and *Fcs* estimated from single profiles (y) we analyzed the slope (m) and the coefficient of determination (R^2) of the linear relation between the different estimates. In absolute values the highest storage was observed at tower C (m = 1.15, R^2 = 0.78) and tower B, m = 1.06, R^2 = 0.80, while the storage at towers A and D was on the average lower (m = 0.96, R^2 = 0.75 and m = 0.83, R^2 = 0.70 respectively). These differences partly reflect the LAI at tower locations, decreasing from towers B (LAI = 2.6) and C (LAI = 2.6) to towers A (LAI = 1.9) and D (LAI = 0.5). For technical reasons, all the towers were placed where the canopy was less dense than the average. There was also a negative relationship between CO_2 accumulation in the canopy air layer and height above sea level, but it was not regular, as already mentioned by *Aubinet et al.* [2005].

5.4.3. CO_2 Turbulent Flux (*Fct*)

[103] Turbulent flux (*Fct*) showed a daily pattern remarkably different for the three flow conditions (Figure 10d). For daytime hours, maximum absolute values of negative turbulent flux were measured during northern and southerly winds, see Table 3. For nighttime hours, turbulent flux showed the highest positive values during the Tramontana, intermediate for southerly winds and lowest during local mountain valley circulation (Table 3).

[104] This nighttime behavior of *Fct* was not followed by soil respiration flux, which on the contrary showed the highest values during the third period (mountain valley wind system), in agreement with soil temperature (Figure 11). This fact cannot be explained from the ecophysiological point of view, but only by the irregular presence of an advective flux, which according to our computations made the largest contribution to the NEE during this period.

[105] Systematic errors in *Fct* occur as a result of instrument accuracy and precision, instrument response time, path length averaging [*Massman and Lee*, 2002; *Loescher et al.*, 2005, 2006] and are also affected by the averaging period for flux computation [*Mann and Lenschow*, 1994; *Sun et al.*, 2007].

[106] The number and types of coordinate rotation also had an impact on calculation of turbulent CO_2 flux. In this study we used a double rotation of coordinates, but for test purposes turbulent fluxes were estimated also without rotation and with three rotations. By not applying rotation, and thus measuring only the component along the geopotential, the sum of turbulent fluxes for the month of July was reduced by 10.3%; on applying three rotations this sum was increased by 4.0%. The detrending also had an effect on *Fct*: on applying linear detrending the sum of *Fct* was reduced by 5.8%.

[107] Averaged data of *Fct* were also influenced by data selection after the quality test for stationarity and ITC characteristics. The nights during the mountain valley wind system period had the highest percentage of excluded data (54.7%) and the highest variation in averaged flux (+30.1%, see Table 3).

5.5. CO_2 Net Ecosystem Exchange

[108] The components of the NEE (*Fca*, *Fcs*, *Fct*) have different diurnal patterns and hence make different contributions to the NEE value (see Figure 12a and Table 3). We defined two data sets representing the NEE: the first, NEEa, where only turbulent and storage fluxes were summed, the second, NEEb, where advective flux was also added (Figure 12b). For the central nighttime hours (2130–0300 LST), *Fca* flux was the largest component of the NEE, with a value approximately twice the one for *Fct*, while the *Fcs* was close to zero. For the transition hours (0530–0800 and 1730–2000 LST) the advective flux was small and positive. The turbulent and storage fluxes were of opposite sign with values on the same order of magnitude. During the daytime (0930–1500 LST) *Fct* was the largest CO_2 flux, *Fca* and *Fcs*, both negative, contributed to higher absolute values of NEE.

[109] Computed NEE values also depend on the number and quality of data used. Table 3 shows the effect of using only data that passed the quality check when estimating turbulent flux. For July 2005, working only with quality assured data, it can be summarized that (1) NEE values were reduced by 53.3% when advective fluxes were added to the turbulent transport term; (2) the contribution of storage flux was negligible.

[110] The accuracy of NEE estimates depends on the accuracy of its single components (*Fct*, *Fcs*, *Fca*) and on the physical requisites allowing their summation. It is to be noted that our *Fct* estimations are based on a traditional, one point setup because of experimental limitations. Thus, they are not coherent with the 3-D setup for the estimation of advective and storage flux. The effect of this simplification on the accuracy of the NEE may be important, since neither the heterogeneity of the sink/source strength nor the turbulent flux divergence is taken into account. An additional source of uncertainty is given by the time delay between the computation period of *Fca*, *Fct*, and that of *Fcs* (see section 4.5.2).

5.6. Impact of CO_2 Advective Term Computation on Ecological Parameter Estimates

[111] The relationships between T_{soil} and NEE at night and between PPFD and NEE during the day can be used as input in the gap-filling process needed to produce annual carbon balance estimates [e.g., *Falge et al.*, 2001], or in process-based ecological modeling of biogeochemical cycles [e.g., *Leuning*, 1995; *Running and Coughlan*, 1988] and are thus of fundamental importance in EC studies.

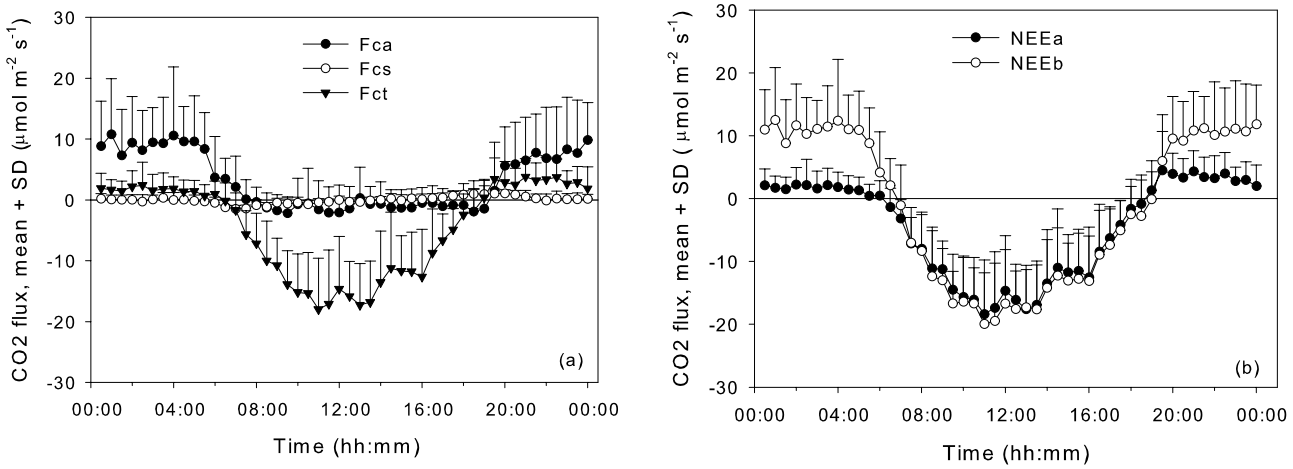

Figure 12. (a) Averaged daily courses of *Fca*, *Fcs*, and *Fct* during the month of July. (b) Averaged daily courses of NEEa and NEEb. Error bars refer to +SD.

[112] The relation between incident PPFD and Net Ecosystem Exchange (NEE) can be described by the modified Michaelis-Menten equation:

$$NEE = -\left(\frac{\alpha \cdot PPFD \cdot F_{\infty}}{\alpha \cdot PPFD + F_{\infty}} - R\right) \quad (22)$$

where F_{∞} is NEE at saturating PPFD, α is apparent quantum yield at ecosystem level, and R is dark respiration. Photosynthetic capacity, F_m, of the vegetation can be defined as NEE at PPFD = 1800 μE m^{-2} s^{-1} [*Ruimy et al.*, 1995].

[113] The same subset (n = 490) of half-hourly values collected during daylight (daylight period was defined when incident PPFD > 2 μE m^{-2} s^{-1}) was used to prepare NEEa and NEEb estimates of net ecosystem exchange (Figure 13). The parameter α was (±95% confidence bounds) 0.04 (±0.01) and 0.09 (±0.03) for NEEa and NEEb respectively, thus indicating a much higher apparent quantum yield in the latter. F_{∞} was respectively 27.7 (±3.2) and 31.3 (±2.4), R was 4.0 (±1.7) and 9.2 (±2.2), thus indicating a much higher dark respiration derived from the NEEb. The correlation coefficient was lower for NEEa (R^2 = 0.54 versus 0.59). F_m (at PPFD = 1800 μE m^{-2} s^{-1}) was similar for the two data sets, −16.2 μmol m^{-2} s^{-1} and −17.1 μmol m^{-2} s^{-1}, thus indicating a slightly higher value for photosynthetic capacity derived from NEEb.

[114] In addition, we tested the deviation from linearity (D) for the two data sets by calculating the difference in R^2 between the Michaelis-Menten equation and a linear model. The values of D were 0.06 for the NEEa and 0.11 for the NEEb data sets, thus indicating that the NEEb data set was characterized by less linearity.

[115] Similar differences in the shape of NEE in relation to PPFD were also found by *Ruimy et al.* [1995] by comparing data sets collected using a micrometeorological method, following *Baldocchi et al.* [1988] and from enclosure experiments, where plants confined in a closed environment showed a higher deviation from linearity in the NEE versus PPFD relation. These differences can be partly explained by different ecophysiological traits affecting plants confined in enclosures or vegetating in free air [*Ruimy et al.*, 1995; *Dore et al.*, 2003]. However, PPFD-NEE relationships similar in shape to those observed in plants growing in enclosures, and to NEEb, were observed also in natural coniferous forests on using the standard EC method [*Röser et al.*, 2002]. Here, the low D found in the NEEa versus PPFD relation appears to be related to limits in the information given by *Fct* and *Fcs* alone. Neglect *Fca* may produce selective systematic errors affecting all the parameters retrieved by the Michaelis-Menten relation.

[116] Total Ecosystem Respiration (TER) is the sum of root, foliage, and woody tissue autotrophic respiration and of soil heterotrophic respiration. Soil Respiration (SR), which is the sum of root autotrophic and soil heterotrophic respiration, is usually the largest ecosystem source of CO_2; foliage and woody tissue respiration generally contribute less than one half to TER [*Lavigne et al.*, 1997; *Law et al.*, 1999; *Granier et al.*, 2000; *Janssens et al.*, 2001; *Ohkubo et al.*, 2007; *Urban et al.*, 2007; *Acosta et al.*, 2008].

[117] *Rodeghiero and Cescatti* [2005] reported an elevated coefficient of determination between T_{soil} and SR on annual basis (R^2 = 0.95) for the Renon site. The reported

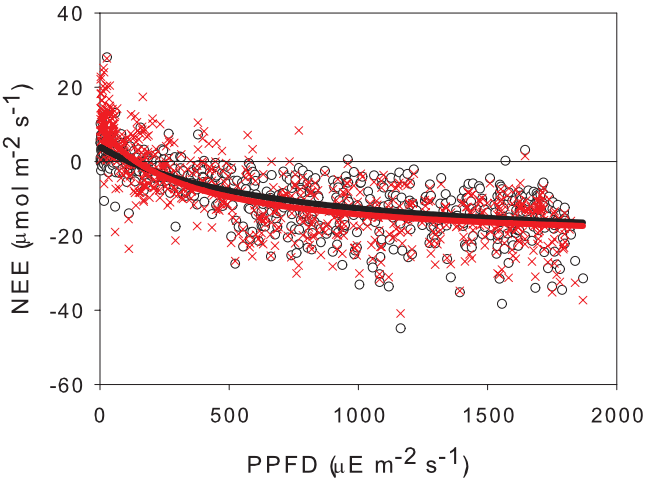

Figure 13. Relation between PPFD and NEEa (black) and NEEb (red).

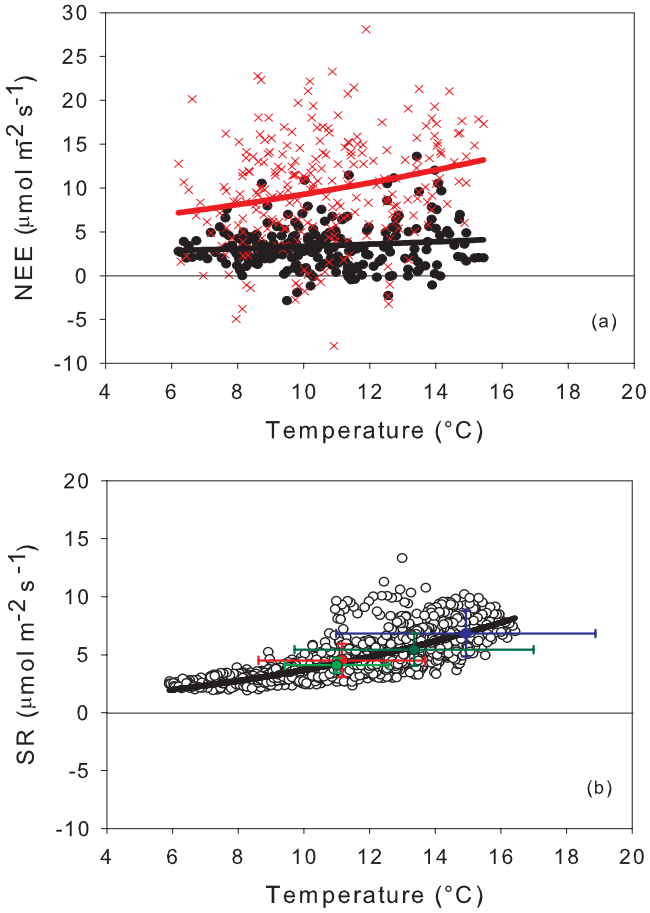

Figure 14. (a) Relation between soil temperature and NEEa (black) and NEEb (red). (b) Relation between soil temperature and CO_2 efflux from the soil, measured during the whole month of July by LI 8100-101 (open black circles) and by LI 6250 during the period 12–14 July. Error bars refer to ±SD. (light green) Waterlogged forest; (dark green) mesophilous young forest; (red) mesophilous adult forest; (blue) clearing.

elevated sensitivity of SR to soil temperature was explained by the narrow thermal excursion along the year. They reported a SR10 value, 5.66, similar to that found for the same site by *Janssens et al.* [2003], SR10 = 4.9, Q10 = 3.4.

[118] Our measurements of soil respiration by the automated chamber Li-8100-101 (LI-COR) during the month of July 2005 confirmed that soil temperature was the single variable that explained most of the pattern of CO_2 evolution from the soil (Figure 14b). The nonlinear regression according to the Q10 function gave values of Q10 = 3.64 and R10 = 3.69. By using the Lloyd and Taylor equation [*Lloyd and Taylor*, 1994], in the formulation of *Falge et al.* [2001]:

$$SR = R_{ref} \cdot \exp(309 \cdot (1/283.15 - T_0) - 1/(T_{soil} + 273.1 - T_0)) \quad (23)$$

parameters R_{ref} and T_0 resulted (mean ± 95% confidence bounds) as 3.67 ± 0.07 and 236.3 ± 1.1 respectively. The coefficient of determination, R^2, was 0.56 for both Q_{10} and Lloyd and Taylor functions.

[119] Data collected inside the reference area in the extensive measuring campaign by the three Li 6250 (LI-COR) chambers, during the period 12–14 July showed that forest types with the widest extension (mature forest, clearings, young forest) gave higher SR values compared to the point chosen for continuous measurements by the automated chamber Li 8100-101. Lower SR values were measured only at the waterlogged locations, where in addition to asphyctic conditions the temperature was lower.

[120] However, the relation between T_{soil} and night NEEa (n = 253) showed a weak correlation and NEEa had averaged values lower than SR measured by the automated chamber Li 8100-101 only (Figure 14a). The relation between T_{soil} and night NEEa, following the Lloyd and Taylor function, was determined by the following values of the parameters: $R_{ref} = 3.3 \pm 0.3$ and $T_0 = 170 \pm 106$, with an R^2 close to zero. The weak correlation can be justified only partly by the intermittence of CO_2 efflux from the soil.

[121] By adding the nonturbulent component (*Fca*) to CO_2 Net Ecosystem Exchange (NEEb) the Lloyd and Taylor parameters were $R_{ref} = 9.0 \pm 0.8$ and $T_0 = 224 \pm 12$ and the coefficient of determination in the relation with soil temperature increased slightly.

[122] NEEa values are therefore inconsistent with results obtained by couvettes at night and are misleading if they are used in ecological functional relations. Although limitations exist, even of a conceptual nature in the approximations introduced, NEE values calculated by adding *Fca* to the sum of *Fct* and *Fcs* (NEEb) are consistent with measurements taken by couvettes, although elevated data scatter still exists.

6. Summary and Conclusions

[123] To overcome theoretical and computational uncertainties related to NEE estimates of turbulent, storage and advection fluxes based on point measurements or along gradients, we tested the hypothesis that the carbon balance in a forest ecosystem may be computed in relation to a control volume unambiguously defined in space by Cartesian coordinates.

[124] We therefore developed a new equation for the CO_2 mass balance based on a fully 3-D approach. Starting from the mass continuity equation, we applied the Gauss transform to obtain the equation that defines advective and turbulent fluxes along the aerial surfaces of the control volume and storage flux inside the same volume. The overall equation obtained (equation (6)) is suitable for mass balance computation of a generic trace gas referred to a defined volume.

[125] The main concern of this study was computation of advective fluxes. The method proposed for their estimation is based on the air mass conservation principle. This implies first a correction of wind and air density values on the surface of the control volume followed by calculation of advection fluxes on this surface. Thus, our approach differs significantly from the NEE methodology commonly applied in the FLUXNET community in two important ways. First, the incompressibility of the mean flow is not assumed a priori. Second, vertical and horizontal advective fluxes are not treated separately, but their sum is computed from values estimated on surface elements of the control volume.

[126] We used the data collected during the Advex campaign at the Renon site (July 2005) to verify to what extent, following this new computational method, we would be able to produce trustworthy NEE estimates at a half-hour time step, an objective that has not yet been reached [*Feigenwinter et al.*, 2008].

[127] To compute advective fluxes, we initially interpolated available measured data of wind velocities and dry air molar density in order to obtain their 3-D fields in the control volume. We then imposed air mass conservation in the control volume by applying a correction factor proportional to the excess/deficit in the dry air mass balance to the normal wind components. The corrected values for wind velocity and dry air density on the external surfaces of the control volume were then used to compute total advective flux (including horizontal and vertical ones). Our analysis, based on the data for July 2005, has shown that advection affects NEE estimates throughout the day and to a different extent in all flow conditions, thus confirming findings by *Sun et al.* [2007].

[128] The mountain slope at Renon enables the development of nocturnal drainage flows during local thermal circulations. Under such conditions, the advective flux was estimated to be 10.8 μmol m^{-2} s^{-1} on the average. The mean nighttime value for the entire month of July was only slightly lower, 8.88 μmol m^{-2} s^{-1}, in the range found by *Marcolla et al.* [2005] (horizontal and vertical advection were both found to be positive, up to 4–5 μmol m^{-2} s^{-1}).

[129] In order to study the impact of advective flux on NEE estimates, we further calculated the turbulent and storage fluxes. Two types of NEE estimates were compared: a more common one [e.g., *Baldocchi et al.*, 1988] where NEE is represented as a sum of only turbulent and storage flux (NEEa) and another one, as proposed in our theoretical framework, NEEb, where advective fluxes were also added.

[130] Despite the simplifications introduced in the calculation of the single terms in the carbon balance equation, NEEb values appeared to be closer to estimates based on the biological activity of the ecosystem studied. The correlation coefficient in the functional relations with soil temperature at night and PPFD during the day was improved when using NEEb. For nighttime hours, only with NEEb was it possible to obtain values of Q10 and R10 approaching the trends of SR obtained by couvette measurements during the experimental campaign, and to have values close to the ones reported for Renon by *Janssens et al.* [2003] and *Rodeghiero and Cescatti* [2005]. For the daytime, the use of NEEb led to a large increase in quantum yield and R dark estimates in the Michaelis-Menten relation.

[131] Our results indicate that the selective systematic error in EC technique induced by advection can be accounted for by direct measurements and that the computation of NEE on a half-hour basis is possible by using the proposed 3-D approach. However, because of the physical limits on the computation of turbulent flux, NEE can be correctly computed only in conditions of stationarity and when ITC conditions are fulfilled [*Foken and Wichura*, 1996]. If we also exclude periods when large deviations from air mass conservation occur, we find that this method requires, besides the standard EC method, a postprocessing procedure of gap filling to produce NEP estimates. Caution must be exercised also when applying the same interpolation algorithms and the same simplifying hypothesis used here to other sites. Phenomena such as storage, which was found to be of slight relevance at the study site, may be relevant in other locations, and must be computed coherently in space and time.

[132] The proposed methodology cannot be applied routinely in all EC sites, because it requires a 3-D design too expensive and difficult to maintain in a long-term perspective. The envisaged use is to set an unbiased reference for evaluating the effectiveness of flow modeling [*Sun et al.*, 2006] and of corrections applied to the EC technique, such as u^* threshold [*Fan et al.*, 1995] or alternative methods [*Van Gorsel et al.*, 2007], to obtain more reliable estimates in the carbon balance and in functional relationships to environmental constraints.

Notation

E	Mole of photons.
Fca	Advective CO_2 flux, μmol m^{-2} s^{-1}.
Fcs	Storage CO_2 flux, μmol m^{-2} s^{-1}.
Fct	Turbulent CO_2 flux, μmol m^{-2} s^{-1}.
n_c	Moles of CO_2 per unit volume, mol m^{-3}.
$\overline{n}_{tot}$	Mole density of dry air including CO_2, mol m^{-3}.
$\overline{p}_a$	Average air pressure (Pa).
NEEa	Net Ecosystem Exchange, $Fcs + Fct$, μmol m^{-2} s^{-1}.
NEEb	Net Ecosystem Exchange, $Fca + Fcs + Fct$, μmol m^{-2} s^{-1}.
R	Universal gas constant (8.3145 J mol^{-1} K^{-1}).
$\overline{r}_c$	CO_2 dry molar fraction, moles of CO_2 to total molecules of dry air (μmol mol^{-1}).
$\overline{r}_{cmoist}$	CO_2 molar fraction, moles of CO_2 to total moles of moist air.
$\overline{r}_{wmoist}$	H_2O molar fraction, moles of H_2O to total moles of moist air.
$\mathbf{S}$	Oriented surface of the control volume (m^2).
$\overline{T}_a$	Average air temperature (K).
T_{soil}	Soil temperature (K).
$\overline{u}$	Average easting wind component (m s^{-1})
$\overline{\mathbf{u}}$	Average wind vector (m s^{-1})
u^*	Friction velocity (m s^{-1})
$\overline{v}$	Average northing wind component (m s^{-1})
V	Reference volume (m^3)
$\overline{w}$	Average vertical wind component (m s^{-1})
ΔQ	Mass variation in the control volume (mol s^{-1})
ΔS_i	Element of aerial surface of the control volume (m^2)
$\overline{\rho}_a$	Average air density (mol m^{-3})
χ	Source or sink of CO_2 (μmol s^{-1})

[133] **Acknowledgments.** The experimental part of this work was performed in the frame of the CarboEurope Integrated Project of the European Commission (contract GOCE-CT-2003-505572). This work was partially supported by The Italian National Research Council (CNR) within the National Consortium of Italian Universities for the Physics of Matter (CNR-CNISM) agreement. National Consortium of Italian Universities for Physics of Atmospheres and the Hydrosphere (CINFAI) is gratefully acknowledged as supporting the activities of the Physics of the Atmosphere Group, Department of Physics, University of Genoa, Italy. Thanks are given for the field work and the helpful suggestions to all the components of the Advex team involved in Renon experiment (M. Aubinet, C. Bernhofer, U. Eichelmann, B. Heinesch, M. Hertel, O. Kolle, J. Kurajdová, F. Lagergren, U. Moderow, R. Queck, and M. Yernaux), to A. Cescatti, G. Hymus, P. Sedlak, and to the personnel of the Renon/Ritten Forest Station. The referees of the first draft of the paper, H. W. Loescher, I. N. Harman, and an anonymous one, are gratefully acknowledged for their detailed and constructive critical review.

References

Acosta, M., M. Pavelka, R. Pokorný, D. Janous, and M. V. Marek (2008), Seasonal variation in CO_2 efflux of stems and branches of Norway spruce trees, *Ann. Bot.*, *101*, 469–477.

Aubinet, M., et al. (2000), Estimates of the annual net carbon and water exchange of forests: The EUROFLUX methodology, *Adv. Ecol. Res.*, *30*, 113–175, doi:10.1016/S0065-2504(08)60018-5.

Aubinet, M., B. Heinesch, and M. Yernaux (2003), Horizontal and vertical CO_2 advection in a sloping forest, *Boundary Layer Meteorol.*, *108*, 397–417, doi:10.1023/A:1024168428135.

Aubinet, M., et al. (2005), Comparing CO_2 storage and advection conditions at night at different CARBOEUROFLUX sites, *Boundary Layer Meteorol.*, *116*, 63–94, doi:10.1007/s10546-004-7091-8.

Baldocchi, D. D., B. B. Hicks, and T. P. Meyers (1988), Measuring biosphere-atmosphere exchanges of biologically related gases with micrometeorological methods, *Ecology*, *69*(5), 1331–1340, doi:10.2307/1941631.

Baldocchi, D., J. J. Finnigan, K. B. Wilson, K. T. Paw U, and E. Falge (2000), On measuring net ecosystem carbon exchange over tall vegetation on complex terrain, *Boundary Layer Meteorol.*, *96*, 257–291, doi:10.1023/A:1002497616547.

Barber, C. B., D. P. Dobkin, and H. T. Hudanpaa (1996), The Quickhull algorithm for convex hulls, *Trans. Math. Software*, *22*, 469–483, doi:10.1145/235815.235821.

Byun, D. W. (1999), Dynamically consistent formulations in meteorological and air quality models for multiscale atmospheric studies. Part II: Mass conservation issues, *J. Atmos. Sci.*, *56*, 3808–3820, doi:10.1175/1520-0469(1999)056<3808:DCFIMA>2.0.CO;2.

Cescatti, A. (2007), Indirect estimates of canopy gap fraction based on the linear conversion of hemispherical photographs: Methodology and comparison with standard thresholding techniques, *Agric. For. Meteorol.*, *143*, 1–12, doi:10.1016/j.agrformet.2006.04.009.

Dore, S., G. J. Hymus, D. P. Johnson, C. R. Hinkle, R. Valentini, and B. G. Drake (2003), Cross validation of open-top chamber and eddy covariance measurements of ecosystem CO_2 exchange in a Florida scrub-oak ecosystem, *Global Change Biol.*, *9*, 84–95, doi:10.1046/j.1365-2486.2003.00561.x.

Falge, E., et al. (2001), Gap filling strategies for defensible annual sums of net ecosystem exchange, *Agric. For. Meteorol.*, *107*, 43–69, doi:10.1016/S0168-1923(00)00225-2.

Fan, S.-M., M. L. Goulden, J. W. Munger, B. C. Daube, P. S. Bakwin, S. C. Wofsy, J. S. Amthor, D. R. Fitzjarrald, K. E. Moore, and T. R. Moore (1995), Environmental controls on the photosynthesis and respiration of a boreal lichen woodland: A growing season of whole-ecosystem exchange measurements by eddy correlation, *Oecologia*, *102*, 443–452, doi:10.1007/BF00341356.

Feigenwinter, C., C. Bernhofer, and R. Vogt (2004), The influence of advection on the short term CO_2-budget in and above forest canopy, *Boundary Layer Meteorol.*, *113*, 201–224, doi:10.1023/B:BOUN.0000039372.86053.ff.

Feigenwinter, C., et al. (2008), Comparison of horizontal and vertical advective CO_2 fluxes at three forest sites, *Agric. For. Meteorol.*, *148*, 12–24, doi:10.1016/j.agrformet.2007.08.013.

Finnigan, J. J. (1999), A comment on the paper by Lee (1998), On micrometeorological observations of surface-air exchange over tall vegetation, *Agric. For. Meteorol.*, *97*, 55–64, doi:10.1016/S0168-1923(99)00049-0.

Finnigan, J. J. (2004a), A re-evaluation of long-term flux measurement techniques. Part 2: Coordinate systems, *Boundary Layer Meteorol.*, *113*, 1–41, doi:10.1023/B:BOUN.0000037348.64252.45.

Finnigan, J. J. (2004b), The footprint concept in complex terrain, *Agric. For. Meteorol.*, *127*, 117–129, doi:10.1016/j.agrformet.2004.07.008.

Finnigan, J. J. (2006), The storage term in eddy flux calculations, *Agric. For. Meteorol.*, *136*, 108–113, doi:10.1016/j.agrformet.2004.12.010.

Finnigan, J. J., and S. E. Belcher (2004), Flow over a hill covered with a plant canopy, *Q. J. R. Meteorol. Soc.*, *130*, 1–29, doi:10.1256/qj.02.177.

Finnigan, J. J., R. Clement, Y. Malhi, R. Leuning, and H. A. Cleugh (2003), A re-evaluation of long-term flux measurement techniques. Part 1: Averaging and coordinate rotation, *Boundary Layer Meteorol.*, *107*, 1–48, doi:10.1023/A:1021554900225.

Foken, T., and B. Wichura (1996), Tools for quality assessment of surface-based flux measurements, *Agric. For. Meteorol.*, *78*, 83–105, doi:10.1016/0168-1923(95)02248-1.

Göckede, M., et al. (2008), Quality control of CarboEurope flux data. Part II: Footprint analyses to evaluate sites in forest ecosystems, *Biogeosciences*, *5*, 433–450.

Goulden, M. L., J. W. Munger, S.-M. Fan, B. C. Daub, and S. C. Wofsy (1996), Measurements of carbon sequestration by long-term eddy covariance: Methods and a critical evaluation of accuracy, *Global Change Biol.*, *2*, 169–182, doi:10.1111/j.1365-2486.1996.tb00070.x.

Granier, A., et al. (2000), The carbon balance of a young beech forest, *Funct. Ecol.*, *14*, 312–325, doi:10.1046/j.1365-2435.2000.00434.x.

Heinesch, B., M. Yernaux, and M. Aubinet (2007), Some methodological questions concerning advection measurements: A case study, *Boundary Layer Meteorol.*, *122*(2), 457–478, doi:10.1007/s10546-006-9102-4.

Janssens, A., et al. (2001), Productivity overshadows temperature in determining soil and ecosystem respiration across European forests, *Global Change Biol.*, *7*, 269–278, doi:10.1046/j.1365-2486.2001.00412.x.

Janssens, I. A., S. Dore, D. Epron, H. Lankreijer, N. Buchmann, B. Longdoz, J. Brossaud, and L. Montagnani (2003), Climatic influences on seasonal and spatial differences in soil CO_2 efflux, in *Canopy Fluxes of Energy, Water and Carbon Dioxide of European Forests*, edited by R. Valentini, pp. 235–256, Ecol. Stud., Springer, Berlin.

Kalnay, E., et al. (1996), The NCEP/NCAR 40-year reanalysis project, *Bull. Am. Meteorol. Soc.*, *77*, 437–471, doi:10.1175/1520-0477(1996)077<0437:TNYRP>2.0.CO;2.

Katul, G. G., J. J. Finnigan, D. Poggi, R. Leuning, and S. E. Belcher (2006), The influence of hilly terrain on canopy-atmosphere carbon dioxide exchange, *Boundary Layer Meteorol.*, *118*, 189–216, doi:10.1007/s10546-005-6436-2.

Kolle, O., and C. Rebmann (2007), Eddysoft: Documentation of a software package to acquire and process eddy covariance data, technical report, 88 pp., Max-Planck-Inst. für Biogeochem., Jena, Germany.

Kowalski, A. S., and P. Serrano-Ortiz (2007), On the relationship between the eddy covariance, the turbulent flux, and surface exchange for a trace gas such as CO_2, *Boundary Layer Meteorol.*, *124*, 129–141, doi:10.1007/s10546-007-9171-z.

Lavigne, M. B., et al. (1997), Comparing nocturnal eddy covariance measurements to estimates of ecosystem respiration made by scaling chamber measurements, *J. Geophys. Res.*, *102*, 28,977–28,986, doi:10.1029/97JD01173.

Law, B. E., M. G. Ryan, and P. M. Anthoni (1999), Seasonal and annual respiration of a ponderosa pine ecosystem, *Global Change Biol.*, *5*, 169–182, doi:10.1046/j.1365-2486.1999.00214.x.

Lee, S. M., S. C. Yoon, and D. W. Byun (2004), The effect of mass inconsistency of the meteorological field generated by a common meteorological model on air quality modeling, *Atmos. Environ.*, *38*, 2917–2926, doi:10.1016/j.atmosenv.2004.02.008.

Lee, X. (1998), On micrometeorological observations of surface-air exchange over tall vegetation, *Agric. For. Meteorol.*, *91*, 39–49, doi:10.1016/S0168-1923(98)00071-9.

Leuning, R. (1995), A critical appraisal of a combined stomatal photosynthesis model for C_3 plants, *Plant Cell Environ.*, *18*, 339–355, doi:10.1111/j.1365-3040.1995.tb00370.x.

Leuning, R. (2007), The correct form of the Webb, Pearman and Leuning equation for eddy fluxes of trace gases in steady and non-steady state, horizontally homogeneous flows, *Boundary Layer Meteorol.*, *123*, 263–267, doi:10.1007/s10546-006-9138-5.

Lloyd, J., and J. A. Taylor (1994), On the temperature dependence of soil respiration, *Funct. Ecol.*, *8*, 315–323, doi:10.2307/2389824.

Loescher, H. W., et al. (2005), Comparison of temperature and wind statistics in contrasting environments among different sonic anemometer–thermometers, *Agric. For. Meteorol.*, *133*, 119–139, doi:10.1016/j.agrformet.2005.08.009.

Loescher, H. W., B. E. Law, L. Mahrt, D. Y. Hollinger, J. Campbell, and S. C. Wofsy (2006), Uncertainties in, and interpretation of, carbon flux estimates using the eddy covariance technique, *J. Geophys. Res.*, *111*, D21S90, doi:10.1029/2005JD006932.

Mahrt, L., D. Vickers, R. Nakamura, M. R. Soler, J. Sun, S. Burns, and D. H. Lenschow (2001), Shallow drainage flow, *Boundary Layer Meteorol.*, *101*, 243–260, doi:10.1023/A:1019273314378.

Mann, J., and D. H. Lenschow (1994), Errors in airborne flux measurements, *J. Geophys. Res.*, *99*(D7), 14,519–14,526, doi:10.1029/94JD00737.

Marcolla, B., A. Cescatti, L. Montagnani, G. Manca, G. Kerschbaumer, and S. Minerbi (2005), Importance of advection in the atmospheric CO_2 exchanges of an alpine forest, *Agric. For. Meteorol.*, *130*, 193–206, doi:10.1016/j.agrformet.2005.03.006.

Massman, W. J., and X. Lee (2002), Eddy covariance flux corrections and uncertainties in long-term studies of carbon and energy exchanges, *Agric. For. Meteorol.*, *113*, 121–144, doi:10.1016/S0168-1923(02)00105-3.

Mauder, M., T. Foken, R. Clement, J. A. Elbers, W. Eugster, T. Grünwald, B. Heusinkveld, and O. Kolle (2008), Quality control of CarboEurope flux data. Part II: Inter-comparison of eddy-covariance software, *Biogeosciences*, *5*, 451–462.

McMillen, R. T. (1988), An eddy correlation technique with extended applicability to non-simple terrain, *Boundary Layer Meteorol.*, *43*, 231–245, doi:10.1007/BF00128405.

Moderow, U., C. Feigenwinter, and C. Bernhofer (2007), Estimating the components of the sensible heat budget of a tall forest canopy in complex terrain, *Boundary Layer Meteorol.*, *123*, 99–120, doi:10.1007/s10546-006-9136-7.

Mölder, M., A. Lindroth, and S. Halldin (2000), Water vapor, CO_2, and temperature profiles in and above a forest: Accuracy assessment of an unattended measurement system, *J. Atmos. Oceanic Technol.*, *17*, 417–425, doi:10.1175/1520-0426(2000)017<0417:WVCATP>2.0.CO;2.

Moncrieff, J. B., Y. Malhi, and R. Leuning (1996), The propagation of errors in long-term measurements of land-atmosphere fluxes of carbon dioxide and water, *Global Change Biol.*, *2*, 231–240, doi:10.1111/j.1365-2486.1996.tb00075.x.

Ohkubo, S., Y. Kosugi, S. Takanashi, T. Mitani, and M. Tani (2007), Comparison of the eddy covariance and automated soil chamber methods for evaluating nocturnal CO_2 exchange in a Japanese cypress forest, *Agric. For. Meteorol.*, *142*, 50–65, doi:10.1016/j.agrformet.2006.11.004.

Pavelka, M., M. Acosta, M. V. Marek, W. Kutsch, and D. Janous (2007), Dependence of the Q(10) values on the depth of the soil temperature measuring point, *Plant Soil*, *292*(1–2), 171–179, doi:10.1007/s11104-007-9213-9.

Paw U, K. T., D. D. Baldocchi, T. P. Meyers, and K. B. Wilson (2000), Correction of eddy-covariance measurements incorporating both advective effects and density fluxes, *Boundary Layer Meteorol.*, *97*, 487–511, doi:10.1023/A:1002786702909.

Poggi, D., and G. G. Katul (2007), Turbulent flows on forested hilly terrain: The recirculation region, *Q. J. R. Meteorol. Soc.*, *133*, 1027–1039, doi:10.1002/qj.73.

Princevac, M., H. J. S. Fernando, and C. D. Whiteman (2005), Turbulent entrainment into natural gravity-driven flows, *J. Fluid Mech.*, *533*, 259–268, doi:10.1017/S0022112005004441.

Raupach, M. R., W. S. Weng, D. J. Carruthers, and J. C. R. Hunt (1992), Temperature and humidity fields and fluxes over low hills, *Q. J. R. Meteorol. Soc.*, *118*, 191–225, doi:10.1002/qj.49711850403.

Rebmann, C., et al. (2005), Quality analysis applied on eddy covariance measurements at complex forest sites using footprint modelling, *Theor. Appl. Climatol.*, *80*, 121–141, doi:10.1007/s00704-004-0095-y.

Rodeghiero, M., and A. Cescatti (2005), Main determinants of forest soil respiration along an elevation/temperature gradient in the Italian Alps, *Global Change Biol.*, *11*, 1024–1041, doi:10.1111/j.1365-2486.2005.00963.x.

Rodeghiero, M., and A. Cescatti (2008), Spatial variability and optimal sampling strategy of soil respiration, *For. Ecol. Manage.*, *255*, 106–112, doi:10.1016/j.foreco.2007.08.025.

Röser, C., L. Montagnani, E.-D. Schulze, D. Mollicone, O. Kolle, M. Meroni, D. Papale, L. Belelli Marchesini, S. Federici, and R. Valentini (2002), Net CO_2 exchange rates in three different successional stages of the "dark taiga" of central Siberia, *Tellus, Ser. B*, *54*, 642–654.

Ruimy, A., P. G. Jarvis, D. D. Baldocchi, and B. Saugier (1995), CO_2 fluxes over plant canopies and solar radiation: A review, *Adv. Ecol. Res.*, *26*, 1–51, doi:10.1016/S0065-2504(08)60063-X.

Running, S. W., and J. C. Coughlan (1988), A general model of forest ecosystem processes for regional applications. I. Hydrologic balance, canopy gas exchange and primary production processes, *Ecol. Modell.*, *42*, 125–154, doi:10.1016/0304-3800(88)90112-3.

Sherman, C. (1978), A mass-consistent model for wind fields over complex terrain, *J. Appl. Meteorol.*, *17*, 312–319, doi:10.1175/1520-0450(1978)017<0312:AMCMFW>2.0.CO;2.

Staebler, R. M., and D. R. Fitzjarrald (2004), Observing subcanopy CO_2 advection, *Agric. For. Meteorol.*, *122*, 139–156, doi:10.1016/j.agrformet.2003.09.011.

Styles, J. M., et al. (2002), Soil and canopy CO_2, $\delta 13CO_2$, H_2O and sensible heat flux partitions in a forest canopy inferred from concentration measurements, *Tellus, Ser. B*, *54*, 768–783.

Sun, H., T. L. Clark, R. B. Stull, and T. A. Black (2006), Two dimensional simulation of airflow and carbon dioxide transport over a forested mountain. Part II: Carbon dioxide budget and advection effects, *Agric. For. Meteorol.*, *140*, 352–364, doi:10.1016/j.agrformet.2006.03.016.

Sun, J. (2007), Tilt corrections over complex terrain and their implication for CO_2 transport, *Boundary Layer Meteorol.*, *124*, 143–159, doi:10.1007/s10546-007-9186-5.

Sun, J., S. P. Burns, A. C. Delany, S. P. Oncley, A. A. Turnipseed, B. B. Stephens, D. H. Lenschow, M. A. LeMone, R. K. Monson, and D. E. Anderson (2007), CO_2 transport over complex terrain, *Agric. For. Meteorol.*, *145*, 1–21, doi:10.1016/j.agrformet.2007.02.007.

Turnipseed, A. A., D. E. Anderson, P. D. Blanken, W. M. Baugh, and R. K. Monson (2003), Airflows and turbulent flux measurements in mountainous terrain. Part 1: Canopy and local effects, *Agric. For. Meteorol.*, *119*, 1–21, doi:10.1016/S0168-1923(03)00136-9.

Turnipseed, A. A., S. Burns, P. D. Blanken, and R. K. Monson (2004), Airflows and turbulent flux measurements in mountainous terrain. Part 2: Mesoscale effects, *Agric. For. Meteorol.*, *125*, 187–205, doi:10.1016/j.agrformet.2004.04.007.

Urban, O., et al. (2007), Ecophysiological controls over the net ecosystem exchange of mountain spruce stand: Comparison of the response in direct vs. diffuse solar radiation, *Global Change Biol.*, *13*, 157–168, doi:10.1111/j.1365-2486.2006.01265.x.

Valentini, R., et al. (2000), Respiration as the main determinant of carbon balance in European forests, *Nature*, *404*, 861–865, doi:10.1038/35009084.

Van Gorsel, E., R. Leuning, H. A. Cleugh, H. Keith, and T. Suni (2007), Nocturnal carbon efflux: Reconciliation of eddy covariance and chamber measurements using an alternative to the u*-threshold filtering technique, *Tellus, Ser. B*, *59*, 397–403, doi:10.1111/j.1600-0889.2007.00252.x.

Vickers, D., and L. Mahrt (2006), Contrasting mean vertical motion from tilt correction methods and mass continuity, *Agric. For. Meteorol.*, *138*, 93–103, doi:10.1016/j.agrformet.2006.04.001.

Webb, E. K., G. I. Pearman, and R. Leuning (1980), Correction of flux measurements for density effects due to heat and water vapour transfer, *Q. J. R. Meteorol. Soc.*, *106*, 85–100, doi:10.1002/qj.49710644707.

Whiteman, C. D. (2000), *Mountain Meteorology, Fundamentals and Applications*, 365 pp., Oxford Univ. Press, Oxford, U. K.

Wilczak, J. M., S. P. Oncley, and S. A. Stage (2001), Sonic anemometer tilt correction algorithms, *Boundary Layer Meteorol.*, *99*, 127–150, doi:10.1023/A:1018966204465.

Xu, L.-K., A. A. Matista, and T. C. Hsiao (1999), A technique for measuring CO_2 and water vapour profiles within and above plant canopies over short periods, *Agric. For. Meteorol.*, *94*, 1–12, doi:10.1016/S0168-1923(99)00004-0.

Xu, L., M. D. Furtaw, R. A. Madsen, R. L. Garcia, D. J. Anderson, and D. K. McDermitt (2006), On maintaining pressure equilibrium between a soil CO_2 flux chamber and the ambient air, *J. Geophys. Res.*, *111*, D08S10, doi:10.1029/2005JD006435.

Yang, B., P. J. Hanson, J. S. Riggs, S. G. Pallardy, M. Heuer, K. P. Hosman, T. P. Meyers, S. D. Wullschleger, and L.-H. Gu (2007), Biases of CO_2 storage in eddy flux measurements in a forest pertinent to vertical configurations of a profile system and CO_2 density averaging, *J. Geophys. Res.*, *112*, D20123, doi:10.1029/2006JD008243.

Yi, C. (2008), Momentum transfer within canopies, *J. Appl. Meteorol. Climatol.*, *47*, 262–275, doi:10.1175/2007JAMC1667.1.

Yi, C., R. K. Monson, Z. Zhai, D. E. Andrson, B. Lamb, G. Allwine, A. A. Turnipseed, and S. P. Burns (2005), Modeling and measuring the nocturnal drainage flow in a high-elevation subalpine forest with complex terrain, *J. Geophys. Res.*, *110*, D22303, doi:10.1029/2005JD006282.

Yi, C., D. E. Anderson, A. A. Turnipseed, S. P. Burns, J. P. Sparks, D. I. Stannard, and R. K. Monsoon (2008), The contribution of advective fluxes to net ecosystem exchange in a high-elevation, subalpine forest, *Ecol. Appl.*, *18*(6), 1379–1390, doi:10.1890/06-0908.1.

M. Acosta, D. Janous, and M. Pavelka, Institute of Systems Biology and Ecology, Academy of Sciences of the Czech Republic, Poříčí 3b, 603 00 Brno, Czech Republic. (manuel@usbe.cas.cz; ejanous@brno.cas.cz; marian@usbe.cas.cz)

E. Canepa, Department of Physics, University of Genova, INFM, CNISM, CNR, Via Dodecaneso 33, I-16146 Genova, Italy. (elisa.canepa@fisica.unige.it)

C. Feigenwinter, Institute of Meteorology, Climatology and Remote Sensing, University of Basel, Klingelbergstrasse 27, CH-4056 Basel, Switzerland. (feigenwinter@metinform.ch)

E. Georgieva, Institute of Geophysics, Bulgarian Academy of Sciences, Acad. G. Bonchev str. bl.3, 1113 Sofia, Bulgaria. (emilia@geophys.bas.bg)

G. Kerschbaumer and L. Minach, Laboratorio di Chimica-Fisica, Agenzia per l'Ambiente, Provincia Autonoma di Bolzano, Via Amba Alagi 5, I-39100 Bolzano, Italy. (guenther.kerschbaumer@provincia.bz.it; luigi.minach@provinz.bz.it)

A. Lindroth and M. Mölder, Department of Physical Geography and Ecosystems Analysis, GeoBiosphere Science Centre, Lund University, Sölvegatan 12, S-223 62 Lund, Sweden. (anders.lindroth@nateko.lu.se; meelis.molder@nateko.lu.se)

G. Manca and G. Seufert, Climate Change Unit, Institute for Environment and Sustainability, TP 050 DG Joint Research Centre, European Commission, Via Fermi 1, I-21020 Ispra (VA), Italy. (giovanni.manca@jrc.it; guenther.seufert@jrc.it)

S. Minerbi and L. Montagnani, Ripartizione Foreste, Provincia Autonoma di Bolzano, Via Brennero 6, I-39100 Bolzano, Italy. (stefano.minerbi@provinz.bz.it; leonar@inwind.it)

M. Zeri, Energy Biosciences Institute, University of Illinois, 1206 West Gregory Drive, Urbana, IL 61801, USA. (mzeri@illinois.edu)

W. Ziegler, Max Planck Institute for Biogeochemistry, P.O. Box 10 01 64, D-07701 Jena, Germany. (wziegler@bgc-jena.mpg.de)